BIOCHEMISTRY
including biophysical chemistry & molecular biology

Article

pubs.acs.org/biochemistry

Homotropic Cooperativity from the Activation Pathway of the Allosteric Ligand-Responsive Regulatory *trp* RNA-Binding Attenuation Protein

Ian R. Kleckner,[†] Craig A. McElroy,[‡] Petr Kuzmic,[§] Paul Gollnick,[∥] and Mark P. Foster*[,†,⊥]

[†]Department of Chemistry and Biochemistry, and Biophysics Program, The Ohio State University, 484 West 12th Avenue, Columbus, Ohio 43210, United States

[‡]College of Pharmacy, The Ohio State University, 500 West 12th Avenue, Columbus, Ohio 43210, United States

[§]BioKin Ltd., 15 Main Street, Suite 232, Watertown, Massachusetts 02472, United States

[∥]Department of Biological Sciences, University at Buffalo, the State University of New York, Buffalo, New York 14260, United States

[⊥]Center for RNA Biology, The Ohio State University, 484 West 12th Avenue, Columbus, Ohio 43210, United States

Supporting Information

ABSTRACT: The *trp* RNA-binding attenuation protein (TRAP) assembles into an 11-fold symmetric ring that regulates transcription and translation of *trp*-mRNA in bacilli via heterotropic allosteric activation by the amino acid tryptophan (Trp). Whereas nuclear magnetic resonance studies have revealed that Trp-induced activation coincides with both microsecond to millisecond rigidification and local structural changes in TRAP, the pathway of binding of the 11 Trp ligands to the TRAP ring remains unclear. Moreover, because each of 11 bound Trp molecules is completely surrounded by protein, its release requires flexibility of Trp-bound (holo) TRAP. Here, we used stopped-flow fluorescence to study the kinetics of Trp binding by *Bacillus stearothermophilus* TRAP over a range of temperatures and observed well-separated kinetic steps. These data were analyzed using nonlinear least-squares fitting of several two- and three-step models. We found that a model with two binding steps best describes the data, although the structural equivalence of the binding sites in TRAP implies a fundamental change in the time-dependent structure of the TRAP rings upon Trp binding. Application of the two-binding step model reveals that Trp binding is much slower than the diffusion limit, suggesting a gating mechanism that depends on the dynamics of apo TRAP. These data also reveal that dissociation of Trp from the second binding mode is much slower than after the first Trp binding mode, revealing insight into the mechanism for positive homotropic allostery, or cooperativity. Temperature-dependent analyses reveal that both binding modes imbue increases in bondedness and order toward a more compressed active state. These results provide insight into mechanisms of cooperative TRAP activation and underscore the importance of protein dynamics for ligand binding, ligand release, protein activation, and allostery.

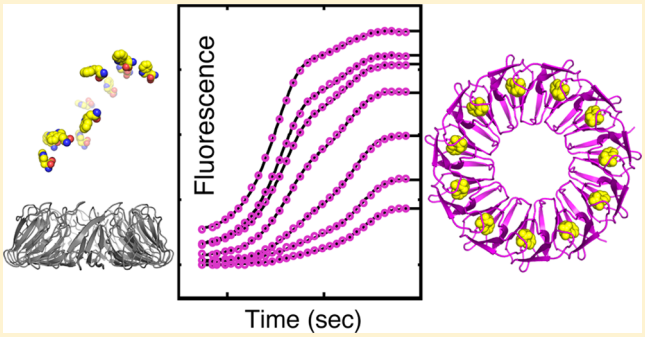

Ligand-responsive proteins are able to regulate essential biological functions because their structure and dynamics are altered via binding to partner molecules.[8] These phenomena are understood not only by comparing different states of the protein but also by describing the pathways that link them. Here, we characterize the activation pathway of the undecameric (11-mer) *trp* RNA-binding attenuation protein (TRAP), which regulates the biosynthesis of the amino acid tryptophan (Trp) in bacilli[9] via a feedback mechanism involving interaction of TRAP with the nascent *trp*-mRNA transcript in response to its ligand, Trp. In the absence of Trp, "apo" TRAP is inactive for binding *trp*-mRNA, which is therefore transcribed in full and translated. When Trp is abundant, up to 11 Trp molecules bind to TRAP, and its "holo" form is active for binding *trp*-mRNA. The binding of TRAP to *trp*-mRNA induces transcription termination prior to the structural genes of the operon, thereby precluding *trp* expression and Trp biosynthesis. TRAP also regulates translation of the *trpE* and *trpD* gene products by altering the accessibility of the mRNA Shine-Dalgarno sequence.[9] Apo TRAP is thought to be inactive for RNA binding because its flexibility masks the RNA-binding site, and Trp binding both rigidifies and alters the local structure of TRAP (Figure 1) such that the target RNA can bind tightly and specifically. This mechanism is supported by several prior studies: (i) nuclear magnetic resonance (NMR) studies that compare the microsecond to millisecond dynamics of apo and holo TRAP,[1,10] (ii)

Received: October 3, 2013
Revised: November 12, 2013
Published: November 13, 2013

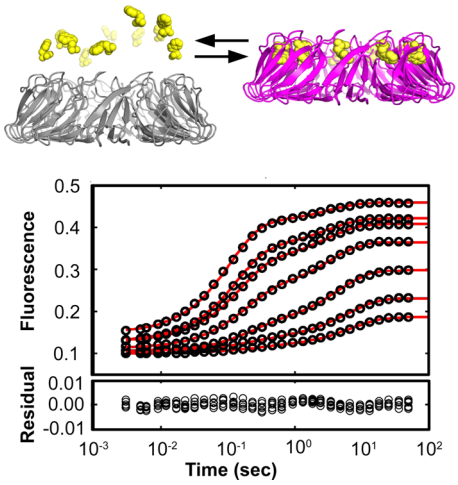

Figure 1. Stopped-flow experiments reveal well-resolved kinetic steps during TRAP activation by Trp binding. In the top panel, apo TRAP is inactive for RNA binding (gray) because of its disordered loops and RNA-binding surface. Undecameric TRAP is activated (magenta) upon binding 11 Trp ligands (yellow), which results in coupled folding and rigidification of the RNA-binding surface. In the bottom panel, the seven transients correspond to 1 μM Trp mixed with 0.1−2.0 μM TRAP 11-mer (1.0−22.3 μM binding sites). These transients were acquired at 25 °C, and similar high-quality data were obtained at seven temperatures in total [15, 20, 25, 30, 35, 40, and 45 °C (Figure S3 of the Supporting Information)]. The red line is the fit to a two-step model describing Trp binding followed by a second Trp binding event (designated the bind−bind or BB model). Although the systematic residuals at ∼1 s suggest an additional kinetic step, the BB model is a prudent simplification, as discussed in the text.

calorimetric experiments that quantify a large decrease in heat capacity upon Trp binding,[11] and (iii) gel mobility shift assays that indicate apo TRAP binds RNA at low temperatures (i.e., conditions under which flexibility is reduced).[12] Crystallographic studies corroborate the disorder of apo TRAP[12] and reveal that holo TRAP forms many specific contacts with Trp,[13,14] RNA,[15] and an inhibitory protein anti-TRAP.[16]

Whereas direct comparisons between the structure and flexibility of the free and bound states reveal features coincident with activation, considering that up to 11 Trp ligands can bind a TRAP ring, the pathway and time course of this activation process are less clear. Moreover, crystallographic data indicate that bound Trp is completely surrounded by protein,[13,14] indicating that its release requires flexibility of holo TRAP. Finally, prior studies of Trp binding homotropic cooperativity have been limited in experimental breadth[11,17] and/or quantitative insight,[18] leaving unresolved the magnitude and mechanism of the effect. Here, we used stopped-flow (SF) fluorescence to monitor binding-associated changes in Trp fluorescence that follow rapid mixing of Trp and apo TRAP from *Bacillus stearothermophilus* (*Bst*) and observed multiple kinetic steps (Figure 1). We then used nonlinear least-squares fitting to test and explore mechanisms that could explain the kinetic observations. Whereas several two- and three-step models were tested, the most parsimonious model that fits the data describes two binding steps. Application of this branched two-binding step model (BB) reveals that Trp binding is much slower than the diffusion limit, which suggests a gating mechanism that depends on the dynamics of apo TRAP. These data also reveal that the second Trp binding event exhibits 1.5-fold faster binding, 100-fold slower dissociation, and thus 150-fold tighter binding than the first Trp binding event, revealing the kinetic mechanism for positive homotropic cooperativity. Furthermore, temperature-dependent analyses indicate that both Trp binding events yield increases in bondedness and order toward the active state. Finally, the rate constants for Trp release reveal that holo TRAP is flexible on the second and millisecond time scale. Interpretation of this two-step model in the context of the undecameric TRAP ring describes a process by which a dynamic protein is initially transiently bound by a subsaturating fraction of ligands, followed by tighter binding by a second set of ligands. This multistep process thus leads to activation of TRAP for RNA binding and subsequent transcriptional and translational repression.

MATERIALS AND METHODS

Sample Preparation. Mutagenesis, expression, and purification of *Bst* A26I TRAP (designated TRAP) were described previously[1] (see the Supporting Information), except that no isotope labeling scheme is utilized here. To accommodate these and other binding experiments, a large stock of TRAP and a large stock of Trp were each stored in reaction buffer [100 mM NaCl, 50 mM $NaPO_4$ (pH 8.0 at 25 °C), and 0.02% NaN_3]. The TRAP stock amounted to 60 mL at 6.82 ± 0.18 μM 11-mer (75 ± 2 μM binding sites), with the concentration measured using the UV absorbance at 280 nm with an ε of 2980 M^{-1} cm^{-1}, calculated using ProtParam.[19] The Trp stock was prepared by adding crystalline Trp (USB Corp.) to buffer matched to the TRAP stock via dialysis, at a concentration of 2030 ± 43 μM based on diluted samples that were quantified by UV absorbance (278 nm; ε = 5579 M^{-1} cm^{-1}).[20] All SF experiments utilized one dilution of Trp (∼200 mL at 1.034 μM) and seven dilutions of TRAP [∼8 mL each at 11-mer concentrations of 0.093, 0.164, 0.323, 0.664, 1.008, 1.350, and 2.027 μM (1.022, 1.800, 3.558, 7.306, 11.088, 14.846, and 22.292 μM binding sites, respectively), designated A−G, respectively]. Because accurate concentrations are essential for analysis, all samples were prepared from their respective stocks with dilution factors measured using an analytical balance that is precise to 0.1 mg (∼0.1 μL).

Stopped-Flow Fluorescence Measurements. SF experiments were performed three to eight times to ensure high-quality data for averaging, using an Applied Photophysics SX.18MV instrument. For each time course, 75 μL of Trp was mixed with an equal volume of TRAP (A−G) or buffer, resulting in 50% dilution of the solutes. Data were acquired in pseudorandom order through the temperature range of the instrument, 15, 20, 25, 30, 35, 40, and 45 °C (also pseudorandomized), for a duration of 50 s (100 s at 15 °C) using 500 points during the first 0.1 s and then 500 points for the remaining time with log time sampling in each segment. The excitation wavelength was 295 ± 5 nm, and the detection range was ≥320 nm, with the photomultiplier tube gain set to 450 V.

Processing Stopped-Flow Data. For each Trp-TRAP concentration and temperature, each time course was smoothed using a third-degree polynomial Savitsky−Golay filter with a five-point window size. Next, at each Trp-TRAP concentration and temperature, the smoothed time courses were averaged (the number of time courses ranged from two to eight; average ± standard deviation of 3.8 ± 1.0; some time courses were removed because of experimental artifacts like air bubbles, and the entire 1.350 μM TRAP time course at 15 °C was

anomalous and therefore discarded completely). Then to allay the effects of photobleaching, apparent especially at higher temperatures, each set of averaged traces was truncated to the time point as soon as the fluorescence signal reached its upper plateau, which occurred after 50, 50, 30, 20, 10, 5, and 5 s for 15, 20, 25, 30, 35, 40, and 45 °C traces, respectively. Finally, the smoothed, averaged, and truncated time courses were resampled with exponential spacing to 30 points per trace to more equally weight the early and late phases of the time course in the subsequent nonlinear fitting analyses. These data processing steps were performed using DYNAFIT version 4.[21,22]

Initial Fits to Stopped-Flow Data. For each Trp-TRAP concentration and temperature, the observed rate constant, k^{Obs}, for each of the kinetic phases was determined by fitting the time-dependent fluorescence signal $F(t)$ to a sum of exponential functions: $F(t) = B + \sum_i^N F_i[1 - \exp(-tk_i^{Obs})]$, where t is time and the fitted parameters are B, the baseline fluorescence, F_i, the fluorescence maximum for phase i, and k_i^{Obs}, the observed rate constant for phase i. Fits to N = 2, 3, and 4 exponential functions were examined for each concentration and temperature (i.e., for each processed stopped-flow trace described above). For each trace, the Bayesian Information Criterion (BIC) was used to assess whether the two-, three-, or four-exponential fit was most appropriate. Nonlinear fitting and the subsequent calculation of the BIC were performed using DYNAFIT.

For each phase and temperature, the relationship between k^{Obs} and TRAP concentration was fit to either (a) the linear equation $k^{Obs}(c_{TRAP}) = k^F c_{TRAP} + k^B$, where c_{TRAP} is the molar concentration of TRAP and k^F and k^B are the forward and reverse kinetic rate constants in units of M^{-1} s^{-1} and s^{-1}, respectively, or (b) the hyperbolic equation $k^{Obs}(c_{TRAP}) = k^F/(1 + k_d/c_{TRAP}) + k^B$, with variable parameters K_d, k^F, and k^B, where K_d is the dissociation constant for the preceding phase and k^F and k^B are the forward and reverse kinetic rate constants, respectively, both in units of s^{-1}.[23] Nonlinear fitting was performed using MATLAB (Mathworks, Inc.).

Testing Kinetic Models. To extend the simplified analysis, stopped-flow data were fit directly to several discrete mechanistic models without simplifying assumptions of pseudo-first-order pre-equilibrium conditions by explicit derivation of appropriate differential equations, followed by numerical integration and iterative nonlinear fitting. DYNAFIT was used to globally fit all time courses for each temperature by specifying the postmixing concentrations of Trp and TRAP for each time course and to perform statistical model testing. For the two-step bind−bind (BB) model selected for further analysis, a pair of binding sites on TRAP (T_T) was modeled that can bind zero, one, or two Trp molecules (W) (Scheme 1).

The fluorescent signal was fit to the sum of ordinary differential equations describing the signal from each species: (1) $d[T\_T]/dt = -2k_1^F[T\_T][W] + k_1^B[T\_TW] + k_1^B[TW\_T]$, (2) $d[W]/dt = -2k_1^F[T\_T][W] + k_1^B[T\_TW] + k_1^B[TW\_T] - k_2^F[T\_TW][W] - k_2^F[TW\_T][W] + 2k_2^B[TW\_TW]$, (3) $d[T\_TW]/dt = k_1^F[T\_T][W] - k_1^B[T\_TW] - k_2^F[T\_TW][W] + k_2^B[TW\_TW]$, (4) $d[TW\_T]/dt = k_1^F[T\_T][W] - k_1^B[TW\_T] - k_2^F[TW\_T][W] + k_2^B[TW\_TW]$, and (5) $d[TW\_TW]/dt = k_2^F[T\_TW][W] + k_2^F[TW\_T][W] - 2k_2^B[TW\_TW]$. The fitted parameters were the four microscopic kinetic rate constants for the forward and reverse paths of each step, k_1^F, k_1^B, k_2^F, and k_2^B, the concentration-dependent fluorescence responses of the Trp-bound species $R(T\_TW) = R(TW\_T)$ and $R(TW\_TW)$, all but one of the TRAP concentrations used (to account for volume delivery errors during stopped-flow experiments), and baseline offsets for each time course. Note that because identical responses and microscopic rate constants are assumed, and are independent of pathway, the branched BB mechanism described above is algebraically identical to an unbranched pathway with a single intermediate state, but we apply a branched pathway because the microscopic rate constants allow us to consider the statistical weights implicit in ligand binding to a molecule with two classes of sites. A similar set of differential equations were derived in an automated fashion for nine other multistep mechanisms using DYNAFIT (see the Supporting Information). Confidence intervals for each fitted parameter were estimated using 1000 iterations of Monte Carlo analysis that refit simulated data that were resampled by shuffling residuals from the best fit to the data,[24] which was implemented in DYNAFIT. Confidence intervals in parameters derived from combinations of kinetic rates (e.g., $K_1 = k_1^F/k_1^B$) were estimated by computing the desired parameter within each of the 1000 Monte Carlo simulations.

Calculation of Encounter Rate Constants. To compare the experimentally observed binding rate to the diffusion limit, we estimated the encounter rate constant between Trp and its binding site on TRAP, as well as upper and lower limits of this value, based on geometric considerations.[25] The upper limit considers TRAP as a sphere, with the encounter rate given by the Smoluchowski equation[26] $k_{Upper} = 4\pi N_0[100R_{Enc}(D_{Trp} + D_{TRAP})]/1000$, where N_0 is Avogadro's number, the factors 100 and 1/1000 yield k_{Upper} in units of M^{-1} s^{-1}, R_{Enc} is the radius of the TRAP sphere that was set to 36 Å based on the holo TRAP crystal structure[15] enlarged by 15% to reflect the more loosely packed apo structure evidenced by diffusion measurements, and D_{Trp} and D_{TRAP} are the diffusion coefficients for Trp and TRAP, respectively, measured as 480×10^{-9} and 5010×10^{-9} cm^2 s^{-1} at 25 °C using dynamic light scattering and NMR, respectively (J. Sachleben, I. Kleckner, and M. Foster, unpublished observations); subsequent analyses assumed 20% uncertainty in each quantity. The temperature dependence of each diffusion constant was estimated from the Stokes−Einstein relation $D(T) = 1000k_BT/[6\pi R_H\eta(T)]$, where k_B is the Boltzmann constant (1.23×10^{-23} J K^{-1}), T is the temperature in kelvin, $\eta(T)$ is the water viscosity at temperature T in N s m^{-2},[27] R_H is the Stokes radius of hydration in meters, and the factor 1000 yields D in units of cm^2 s^{-1}. The lower limit of the encounter rate is given by the Solc and Stockmayer equation[28] $k_{Lower} = k_{Upper}A_{bind}/(4\pi R_{Enc}^2)$, which reduces k_{Upper} to account for the area of the Trp-binding sites on TRAP, A_{bind}. Because of the lack of high-resolution structural details of apo TRAP, A_{bind} was estimated using the minimal cross-sectional area of a 11.1 Å × 7.5 Å × 7.2 Å rectangular prism that encloses the van der Waals representation of a Trp molecule (i.e., 7.5 Å × 7.2 Å = 54 $Å^2$, which is the smallest area through which a single Trp molecule could fit). For the first Trp binding, A_{bind} = 11 × 54 $Å^2$ = 594 $Å^2$ because there are 11 free sites per donut; for the second Trp

Scheme 1

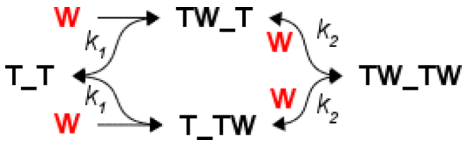

dx.doi.org/10.1021/bi401364v | Biochemistry 2013, 52, 8855−8865

binding, $A_{bind} = 6 \times 54$ Å$^2 = 324$ Å^2 because there are six free sites per donut (i.e., assuming that the first first Trp binding steps have no neighboring Trp molecules and the second Trp binding steps have one or two neighboring Trp molecules). An intermediate value of the encounter rate constant is given by the Shoup equation[25] $k_{Intermed} = k_{Upper}[(A_{bind}/\pi)/(\pi R_{Enc})]^{1/2}$, which reduces the upper limit to account for A_{bind} but is greater than the lower lower limit to account for rotational diffusion of TRAP, which effectively presents the binding area as being larger than its geometric fraction. The probability of Trp binding upon encounter was calculated as the ratio of the observed rate constant for binding to any single site, k_1^F, to the calculated rate constant for encounter with any single site: $Pr(Bind) = k_1^F/k_{Enc}$, where k_{Enc} is equal to k_{Lower}, k_{Upper}, or $k_{Intermed}$.

Extended Arrhenius Analysis Using the Temperature Dependence of Rate Constants. To thermodynamically describe three ground states, T_T, T_TW (and TW_T), and TW_TW, and the two transition states, $[T\_TW]^‡$ and $[TW\_TW]^‡$, the temperature dependence of fitted rate constants was subjected to Arrhenius analysis using the extended relation, which includes a non-zero transition state heat capacity change, $\Delta C_p^‡$, as implied by curvature in the Arrhenius plots:[29,30]

$$\ln\left[\frac{k(T)}{k(T_0)}\right] = \frac{\Delta H_0^‡}{RT_0} - \frac{1}{RT}\left\{\Delta H_0^‡ + \Delta C_p^‡ \left[T - T_0 - T\ln\left(\frac{T}{T_0}\right)\right]\right\} \quad (1)$$

where $k(T)$ is the fitted rate constant from the SF data at absolute temperature T, with reference temperature T_0 of 298 K used to compare dimensionless quantities among all the steps;[31] R is the gas constant (1.985 cal K^{-1} mol^{-1}); $\Delta H_0^‡$ is the activation enthalpy at T_0 with $\Delta H^‡(T) = \Delta H_0^‡ + \Delta C_p^‡(T - T_0)$; and $\Delta C_p^‡$ is the activation heat capacity, assumed to be independent of temperature. For each of four steps, the fitted rate constants $k(T)$ at seven temperatures were fit to eq 1 using MATLAB to extract either (a) only $\Delta H_0^‡$, while $\Delta C_p^‡$ was fixed to zero, or (b) both $\Delta H_0^‡$ and $\Delta C_p^‡$, if $\Delta C_p^‡$ was allowed to be non-zero. Although introducing non-zero values of $\Delta C_p^‡$ did not result in statistically significant improvements in fits for all rate constants (Figure S4 of the Supporting Information), these were employed to retain consistency with both the principle of microscopic reversibility and results from van't Hoff analysis (below). Note that the sign of $\Delta C_p^‡$ was inverted from ref 30 for consistency in obtaining ground state thermodynamic quantities from their transition state counterparts (i.e., to ensure that $X^{GS} = X_F^‡ - X_B^‡$, where $X = G$, H, S, or C_p, and X^{GS} designates a ground state quantity). Using $\Delta H_0^‡$, the relative reference activation entropy was obtained at temperature T_0:

$$\Delta S_{0,Rel}^‡ = R\ln[k(T_0)] + R\ln\left(\frac{h}{k_B}\right) + R\ln\left(\frac{1}{T_0}\right) + \frac{1}{T_0}\Delta H_0^‡ - R\ln(\kappa) \quad (2)$$

where h is Planck's constant (6.626×10^{-34} J s), k_B is the Boltzmann constant (1.23×10^{-23} J K^{-1}), and κ is the transmission coefficient. Here, $\Delta S_{0,Rel}^‡$ was estimated using $\kappa = 1$, even though this violates the assumption of reversibility in the reaction mechanism,[29] yielding a theoretical upper limit for activation entropies and therefore a lower limit for activation free energies ($\Delta G_{0,Min}^‡ = \Delta H_0^‡ - T\Delta S_{0,Max}^‡$). Moreover, although $\Delta S_{0,Rel}^‡$ is offset by an amount $R \times \ln(\kappa)$ and therefore is inaccurate to the extent that $\kappa < 1$,[29] differences (but not ratios) in stepwise $\Delta S_{0,Rel}^‡$ values are accurate because factors of $R \times \ln(\kappa)$ are subtracted away. Confidence intervals in these fitted parameters were estimated using 10000 iterations of Monte Carlo resampling. Specifically, for each of 10000 iterations, one data point at each temperature was randomly sampled from the 1000 Monte Carlo fits used to generate confidence intervals in kinetic rate constants at that temperature (mentioned above). In this way, an across-temperature simulated data set was generated and fit 10000 times.

Extended van't Hoff Analysis Using the Temperature Dependence of Equilibrium Constants. In the Arrhenius analysis, the $\Delta S_{0,Max}^‡$ values were lower limits and the $\Delta G_{0,Min}^‡$ values were upper limits because the value of transmission coefficient κ in eq 2 is not known but was assumed to be the maximal value of 1. In the van't Hoff analysis, this limitation is circumvented because equilibrium constants are ratios of rate constants (or differences in $\Delta G^‡$), and therefore, the κ term is removed. Specifically, the equilibrium constants are $K_i = k_i^F/k_i^B = \exp(-\Delta G_i/RT)$ for step i (1 or 2). Like the Arrhenius analyses, the extended form of the van't Hoff relation was used to compare fits of the data using (a) ΔC_p fixed to zero and (b) ΔC_p optimized to a non-zero value during fitting:[32]

$$\ln\left[\frac{K(T)}{K(T_0)}\right] = \frac{\Delta H_0 - T_0\Delta C_p}{R}\left(\frac{1}{T_0} - \frac{1}{T}\right) + \frac{\Delta C_p}{R}\ln\left(\frac{T}{T_0}\right) \quad (3)$$

where $K(T)$ is each equilibrium constant obtained from fits to the SF data at absolute temperature T, with reference temperature $T_0 = 298$ K used to compare dimensionless quantities among all the steps;[31] R is the gas constant (1.985 cal K^{-1} mol^{-1}); ΔH_0 is the enthalpy at T_0 with $\Delta H(T) = \Delta H_0 + \Delta C_p(T - T_0)$; and ΔC_p is the temperature-independent heat capacity. For each of three equilibria, the input data $K(T)$ were supplied at seven temperatures and fit to eq 3 using MATLAB to either (a) only ΔH_0, while ΔC_p was fixed to zero, or (b) both ΔH_0 and ΔC_p, if ΔC_p was allowed to be non-zero. Confidence intervals in these fitted parameters were estimated using 10000 iterations of Monte Carlo resampling as described above for Arrhenius analyses. For ground state quantities, the following relations were used to obtain thermodynamic quantities at nonreference temperatures: $\Delta G(T) = -RT\ln[K(T)]$, $\Delta H(T) = \Delta H(T_0) + \Delta C_p(T - T_0)$, and $\Delta S(T) = (\Delta H - \Delta G)/T$.

RESULTS

Trp Binding to TRAP Occurs in Multiple Kinetic Steps. To characterize the time-dependent pathway for Trp binding and TRAP activation, we used a stopped-flow (SF) apparatus to rapidly mix Trp and apo TRAP[a] in solution while measuring the time-resolved fluorescence of Trp, which is sensitive to its local electronic environment (Figure 1);[33] the TRAP protein itself possesses no tryptophan residues, which would complicate the interpretation of data. Each of ~49 fluorescence time courses was acquired using a fixed concentration of Trp mixed with one of seven concentrations of TRAP acquired at one of seven temperatures between 15 and 45 °C (Figure S3 of the Supporting Information). These data clearly demonstrated that Trp binding occurs through at least two time-resolved steps,

with time constants ranging from ~0.1 to ~10 s (Figure 1). Mechanistically, because these data reflect changes in bulk Trp fluorescence, the observed steps could report structural changes in TRAP related to its activation (i.e., isomerization) and/or multiple Trp binding events, because each TRAP oligomer can bind up to 11 Trp molecules.

At most of the temperatures and TRAP concentrations sampled, the major features of the binding curves could be captured by a two-step process described by a two-phase exponential function, although additional kinetic steps are implied by the nonrandom small residuals (Figure 1). Indeed, a three-step process is statistically preferred over a two-step or four-step process when comparing two-, three-, and four-phase exponential functions in their ability to fit the data (Figure S1 and Table S3 of the Supporting Information). As discussed below, although at least one additional step is implicit in the binding mechanism, we proceed with a two-step model for quantitative analyses of fitted rate constants because the two-step model captures most of the features of the data, and more complex models yield poorly constrained fitted parameters.

A Two-Step Kinetic Model for Binding of Trp to TRAP. To learn more about the mechanisms of the kinetic steps evident in the data, we explored the concentration dependence of the apparent rate constants obtained from fitting the two- and three-phase exponential decay functions (a four-phase exponential fit is not discussed further because it is too complex, as mentioned above). The two-phase analysis revealed a nearly linear relationship between k_1^{Obs} and TRAP concentration, while k_2^{Obs} exhibits a hyperbolic relationship to TRAP concentration (Figure 2 and Figure S2 of the Supporting Information). These relationships are consistent with a mechanism in which the second step involves the product of the first step. The three-phase analysis suggests that an additional step occurs between the first and second steps from the two-phase analysis [i.e., two-phase steps 1 and 2 correspond to three-phase steps 1 and 3, respectively (Figure S2 of the Supporting Information)]. Although estimates of microscopic forward and reverse rate constants can be obtained by assuming linear and hyperbolic dependencies of the apparent rate constants for the kinetic phases (Table S2 of the Supporting Information), we obtained more accurate forward and reverse rate constants by globally fitting data to differential equations via numerical integration because not all of the data were recorded under simplifying pseudo-first-order conditions.

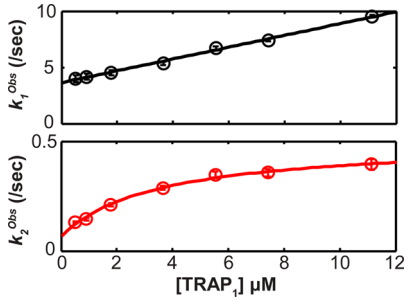

Figure 2. Concentration dependencies of the mechanism-independent apparent rate constants for a two-step process reveal that the second step mechanistically follows the first. In the top panel, the faster (first) step exhibits a linear relationship between k^{Obs} and the total TRAP concentration, [TRAP]. In the bottom panel, the second (slower) step exhibits a hyperbolic relationship between k^{Obs} and [TRAP]. These data correspond to 25 °C and are corroborated by data at other temperatures (Figure S2 and Table S2 of the Supporting Information). Error bars show the standard errors from fitting the time-dependent SF data to a two-phase exponential function. This behavior supports analysis of the data using a two-step mechanism.

To identify the best mechanism for describing these data, several candidate mechanisms were fit to the data by numerical integration of differential equations that arise from each mechanism, each of which included two or three binding and/or isomerization steps (see the Supporting Information).[b] We used DYNAFIT to globally fit the six or seven TRAP concentrations within each temperature and to statistically compare mechanistic models. As discussed in the Supporting Information, we found the two-step BB model to best describe the data (Scheme 1). The BB model describes binding of Trp to a pair of binding sites (T_T) using four microscopic rate constants: (1) k_1^F for the first Trp binding

$$T\_T + W \xrightarrow{k_1^F} T\_TW$$

and

$$T\_T + W \xrightarrow{k_1^F} TW\_T$$

(2) k_1^B for the first Trp release

$$T\_TW \xrightarrow{k_1^B} T\_T + W$$

and

$$TW\_T \xrightarrow{k_1^B} T\_T + W$$

(3) k_2^F for the second Trp binding

$$T\_TW + W \xrightarrow{k_2^F} TW\_TW$$

and

$$TW\_T + W \xrightarrow{k_2^F} TW\_TW$$

and (4) k_2^B for the second Trp release

$$TW\_TW \xrightarrow{k_2^B} T\_TW + W$$

and

$$TW\_TW \xrightarrow{k_2^B} TW\_T + W$$

The model also includes parameters related to how each molecular species contributes to the observed fluorescence data, and it accounts for volume delivery errors (see Materials and Methods). In TRAP, because the ligand-binding sites are equivalent, differences in the rate constants for first and second binding events imply allosteric coupling between binding sites.

The Tighter Second Trp Binding Reveals the Mechanism of Homotropic Allostery. To assess the degree of cooperativity between the first and second Trp binding modes, we compared the binding and dissociation rate constants (k_i^F and k_i^B, respectively) and affinities ($K_1 = 1/K_{d1} = k_1^F/k_1^B$, and $K_2 = 1/K_{d2} = k_2^F/k_2^B$) of the first and second binding steps (Table 1). The microscopic rate constant for the second Trp binding mode is moderately faster (1.4–2.5-fold) than that of the first, indicating that Trp binding exhibits modest positive cooperativity in a kinetic sense (i.e., activation free energy $\Delta G^{\ddagger}$ decreases after the first binding). However, a much greater difference was found in the rate constants for dissociation (k_1^B and k_2^B), which differ by 2 orders of

dx.doi.org/10.1021/bi401364v | Biochemistry 2013, 52, 8855–8865

Table 1. Fitted Parameters from Analysis of Kinetic Data Using the BB Model[a]

T (°C)	k_1^F (μM^{-1} s^{-1})	k_1^B (s^{-1})	k_2^F (μM^{-1} s^{-1})	k_2^B (s^{-1})	R(T_TW)	R(TW_TW)	K_{d1} (μM)	K_{d2} (μM)	K_2/K_1
15	0.23 [0.22, 0.24]	0.97 [0.92, 1.03]	0.33 [0.30, 0.36]	0.011 [0.010, 0.012]	0.75 [0.74, 0.77]	1.37 [1.35, 1.39]	4.25 [3.99, 4.54]	0.033 [0.029, 0.037]	128 [110, 154]
20	0.34 [0.34, 0.35]	1.80 [1.73, 1.88]	0.52 [0.49, 0.56]	0.018 [0.017, 0.019]	0.78 [0.76, 0.80]	1.35 [1.34, 1.36]	5.23 [4.98, 5.51]	0.034 [0.031, 0.037]	153 [134, 173]
25	0.51 [0.50, 0.52]	3.52 [3.37, 3.68]	0.80 [0.75, 0.85]	0.036 [0.035, 0.038]	0.84 [0.82, 0.87]	1.36 [1.35, 1.38]	6.93 [6.53, 7.32]	0.045 [0.042, 0.049]	153 [133, 175]
30	0.65 [0.63, 0.67]	6.87 [6.63, 7.13]	1.20 [1.13, 1.28]	0.077 [0.075, 0.080]	0.88 [0.85, 0.92]	1.34 [1.32, 1.35]	10.57 [9.99, 11.16]	0.064 [0.060, 0.069]	164 [145, 186]
35	0.83 [0.79, 0.86]	13.30 [12.83, 13.78]	1.70 [1.58, 1.84]	0.171 [0.166, 0.176]	0.94 [0.89, 0.99]	1.33 [1.31, 1.35]	16.03 [15.02, 17.22]	0.100 [0.092, 0.109]	160 [138, 188]
40	1.01 [0.92, 1.08]	24.04 [22.96, 25.13]	2.14 [1.84, 2.49]	0.420 [0.403, 0.435]	0.93 [0.84, 1.05]	1.34 [1.29, 1.40]	23.91 [21.23, 27.26]	0.196 [0.164, 0.231]	122 [92, 167]
45	1.18 [0.80, 1.48]	48.52 [45.01, 52.25]	2.93 [2.04, 4.80]	0.879 [0.834, 0.928]	1.08 [0.83, 1.66]	1.35 [1.21, 1.53]	41.12 [30.69, 64.00]	0.300 [0.177, 0.442]	137 [70, 359]

[a]The kinetic parameters k_1^F, k_1^B, k_2^F, and k_2^B correspond to the kinetic steps of the first Trp binding, first Trp release, second Trp binding, and second Trp release, respectively. The two "response" parameters, R(T_TW) and R(TW_TW), are proportional to the quantum yield of the bound states. The units of k_1^F and k_2^F correspond to the concentration of TRAP-binding sites (i.e., 11 times [$TRAP_{11}$]); 95% confidence intervals estimated using Monte Carlo analyses are given in brackets. $K_2/K_1 = K_{d1}/K_{d2}$ and is the ratio of the equilibrium association constants obtained from the ratios of the forward and backward rate constants ($K_i = k_i^F/k_i^B$).

magnitude (Table 1); the data indicate that ligand dissociation after the second binding mode is ~100 times slower than after the first mode. Consequently, the affinity of the second Trp binding is ~150 times tighter than the affinity of the first Trp binding, indicating that Trp binding is positively cooperative in a thermodynamic sense (i.e., binding free energy ΔG decreases after the first binding).

Trp Binding Is Much Slower Than the Diffusion Limit. The observed rate constant for first and second Trp binding, k_1^F and k_2^F, respectively, ranged from 0.22 to 2.9 μM^{-1} s^{-1} from 15 to 45 °C. To compare k_1^F and k_2^F with the diffusion-limited encounter rate constant between Trp and its binding site on TRAP, the area of the binding site is estimated as the minimal cross-sectional area of Trp, and two additional geometric considerations provide upper and lower limits for the sake of comparison[25] (Figure 3a). Upon dividing the binding rates by the encounter rates at each temperature, we find that Trp binding upon encounter is highly unlikely, with an only 0.016–0.136% chance of binding upon encounter [i.e., only 1 in 6000 to 1 in 700 (Figure 3b)]. Such unproductive collisions imply a large population of conformations that do not favor binding, through either occlusion or poor complementarity, and that binding-permissive conformations are sampled rarely.

Arrhenius Analysis Reveals a Stepwise Reduction in Heat Capacity upon Binding of Trp to TRAP. To gain structural insight into the two binding steps, the temperature dependencies of the four kinetic rate constants from the BB model are interpreted using an extended Arrhenius analysis. The analysis yields the activation enthalpies ($\Delta H^{\ddagger}$), heat capacities ($\Delta C_p^{\ddagger}$), minimal entropies ($\Delta S_{0,Min}^{\ddagger}$), and maximal free energies ($\Delta G_{0,Max}^{\ddagger}$)[30,34] (Table 2 and Figure 4) that compare each of the ground state and transition state structures. Data at 45 °C were not included in the Arrhenius or van't Hoff temperature-dependent analyses, as the fitted rate constant values were outlying and poorly defined at this temperature (Figure S6 of the Supporting Information). The curvature in the Arrhenius plots require the use of a non-zero $\Delta C_p^{\ddagger}$ term (Figure 4 and Figure S4 of the Supporting Information), which implies a change in both the extent of the conformations sampled and the solvent-accessible surface area[35] between the ground states and transition states. The

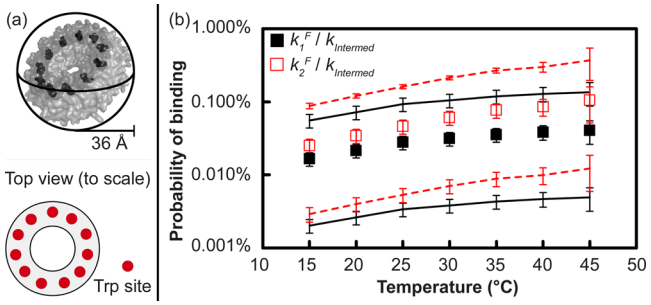

Figure 3. Low probability of Trp binding upon encounter with TRAP implies ligand gating. (a) Three geometric considerations of TRAP determine upper and lower limits of the Trp–TRAP encounter rate constants. The upper limit considers TRAP as a sphere; the lower limit reduces this value to account for the area of the Trp-binding sites (11 red circles), and the intermediate value increases the lower limit to account for rotational diffusion of TRAP, which effectively presents the active area as being larger than its geometric value. (b) The probability of binding upon encounter is obtained by dividing the observed binding rate constant, k_1^F or k_2^F, by the calculated encounter rate constant, k_{Enc}; this indicates an only 0.016–0.136% chance of binding upon encounter (i.e., only 1 in 6000 to 1 in 700), which increases at higher temperatures. Black and red squares indicate the binding probabilities for binding steps 1 and 2, respectively, while the lines indicate upper and lower limits of binding probability, as calculated using lower and upper limits of the encounter rate constant (see Materials and Methods). Error bars are propagated from 95% confidence intervals for k_1^F and k_2^F and uncertainties in geometric quantities. The probability of the second binding is slightly higher than that of the first binding, reflecting the fact that k_2^F is greater than k_1^F and that fewer empty sites are available for the second binding.

analysis reveals similar negative $\Delta C_p^{\ddagger}$ values for the forward reactions, k_1^F and k_2^F (−404 and −335 cal mol^{-1} K^{-1}, respectively), likely reflecting similar changes in solvation during the binding process. A much larger $\Delta C_p^{\ddagger}$ is observed for k_2^B (702 cal mol^{-1} K^{-1}) than for k_1^B (104 cal mol^{-1} K^{-1}), indicating that dissociation from the fully bound state involves an intermediate with substantially increased surface exposure and conformational diversity. The analysis reveals that the pathway for binding of Trp to TRAP proceeds via intermediates with reduced C_p, and that dissociation from the

dx.doi.org/10.1021/bi401364v | Biochemistry 2013, 52, 8855–8865

Table 2. Extended Arrhenius Analysis Fit Results (T_0 = 25 °C)[a]

	step 1		step 2	
thermodynamic term	forward	backward	forward	backward
$\Delta H_0^{\ddagger}$ (kcal mol^{-1})	11.7 [11.0, 11.8]	22.8 [22.3, 23.6]	13.5 [13.1, 15.2]	25.2 [23.8, 25.4]
$\Delta C_p^{\ddagger}$ (cal mol^{-1} K^{-1})	−404 [−527, −349]	104 [40, 256]	−335 [−428, −23]	702 [640, 889]
$\Delta S_{0,\mathrm{Min}}^{\ddagger}$ (cal mol^{-1} K^{-1})	108 [105, 108]	121 [120, 124]	114 [113, 120]	120 [116, 121]
$\Delta G_{0,\mathrm{Max}}^{\ddagger}$ (kcal mol^{-1})	−20.4 [−20.4, −20.4]	−13.4 [−13.4, −13.3]	−20.6 [−20.7, −20.6]	−10.7 [−10.7, −10.6]

[a]The thermodynamic terms $\Delta H_0^{\ddagger}$, $\Delta C_p^{\ddagger}$, $\Delta S_{0,\mathrm{Min}}^{\ddagger}$, and $\Delta G_{0,\mathrm{Max}}^{\ddagger}$ refer to the activation enthalpy, activation heat capacity, minimal activation entropy, and maximal activation free energy, respectively. The values of $\Delta H_0^{\ddagger}$ and $\Delta C_p^{\ddagger}$ are obtained by fitting the temperature dependence of the kinetic rates (Table 1) to the extended Arrhenius equation (eq 1). The values of $\Delta S_{0,\mathrm{Min}}^{\ddagger}$ and $\Delta G_{0,\mathrm{Max}}^{\ddagger}$ are obtained using $\Delta H_0^{\ddagger}$ in eq 2 and the relations in Materials and Methods; 95% confidence intervals estimated using Monte Carlo analyses are given in brackets.

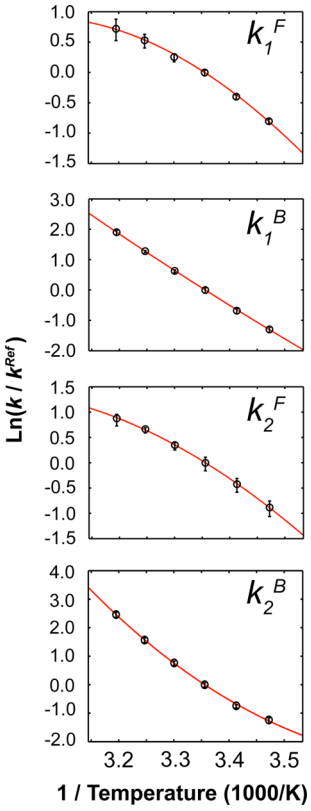

Figure 4. Extended Arrhenius analysis reveals the magnitude of the heat capacity change for activation, $\Delta C_p^{\ddagger}$, that allows binding of Trp to TRAP. The curvature in the Arrhenius plots describes the magnitude and sign of the activation $\Delta C_p^{\ddagger}$ between the ground state and transition states for each step. Error bars are 95% confidence intervals from a Monte Carlo error analysis propagated from the original stopped-flow time courses. Negative values in the forward direction are indicated by convex curves, while positive values of the reverse steps are determined by concave curves. $\Delta C_p^{\ddagger}$ is largest for binding of Trp to TRAP and dissociation of fully bound TRAP, k_2^B, indicating that those transitions involve larger changes in structure and solvation.

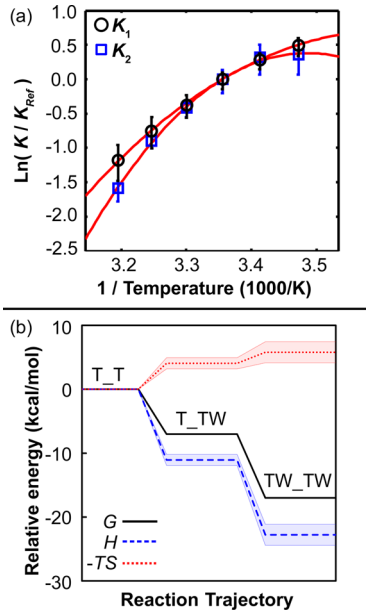

Figure 5. Extended van't Hoff analysis reveals a stepwise increase in bondedness and order of the Trp−TRAP−solvent system upon Trp binding. (a) The van't Hoff plot illustrates curvature for both steps, which are each fit with slope ΔH and curvature ΔC_p. Error bars are 95% confidence intervals from a Monte Carlo error analysis propagated from the original stopped-flow time courses. (b) Energetic contributions from enthalpy H and entropy $-TS$ at 25 °C along the reaction coordinate reveal that increased bondedness and order accompany favorable binding free energy G. The energy of free state T_T is set to zero for reference, and the shaded regions enclose 95% confidence intervals from Monte Carlo analysis for obtaining G, H, and $-TS$ via ΔH and ΔC_p from the extended van't Hoff analysis.

doubly bound state involves structural rearrangements much larger than those seen for the singly bound states.

van't Hoff Analysis Reveals That Both Binding Steps Increase Bondedness and Order. Ground state free energies G and entropies S were quantified by using the fitted rate constants to derive equilibrium constants and subjecting these to extended van't Hoff analysis,[32] which yields ΔG and $T\Delta S$ in addition to ΔH and ΔC_p (Figure 5a, Figure S5 of the Supporting Information, and Table 3). As shown from the reaction coordinate plot (Figure 5b), both binding steps exhibit favorable changes in free energy and enthalpy, but an unfavorable loss of entropy ($\Delta G < 0$, $\Delta H < 0$, and $-T\Delta S > 0$). This reflects a stepwise increase in bondedness and order along the reaction coordinate, thus distinguishing the singly and doubly bound states. Furthermore, as the temperature increases from 15 to 45 °C, Trp binding is favored less [K_{d1} and K_{d2} increase (Table 1)].

DISCUSSION

Binding of Trp to TRAP Proceeds via a Well-Defined Kinetic Intermediate. *In vitro* transcription assays indicate that the kinetics of RNA binding are important determinants for the effectiveness of transcription attenuation,[36] thus drawing attention to the kinetics of TRAP activation via Trp binding. Stopped-flow fluorescence experiments reported here reveal that the kinetics of binding of Trp to TRAP proceed via at least two well-separated kinetic steps. We have applied a two-step BB

dx.doi.org/10.1021/bi401364v | Biochemistry 2013, 52, 8855−8865

Table 3. Extended van't Hoff Analysis Fit Results (T_{Ref} = 25 °C)[a]

thermodynamic term	step 1 (first binding)	step 2 (second binding)
ΔH_0 (kcal·mol^{-1})	−11.1 [−12.4, −10.7]	−11.7 [−11.9, −9.1]
ΔC_p (cal mol^{-1} K^{-1})	−506 [−751, −419]	−1048 [−1240, −736]
ΔS_0 (cal mol^{-1} K^{-1})	−13.6 [−18.0, −12.2]	−5.8 [−6.4, 3.0]
ΔG_0 (kcal mol^{-1})	−7.0 [−7.1, −7.0]	−10.0 [−10.1, −10.0]

[a]The thermodynamic terms ΔH_0, ΔC_p, ΔS_0, and ΔG_0 refer to the enthalpy, heat capacity, entropy, and free energy, respectively. These values of ΔH_0 and ΔC_p are obtained by fitting the temperature dependence of the equilibrium constants (Table 1) to the extended van't Hoff equation (eq 3). The values of ΔS_0 and ΔG_0 are obtained using additional equations described in Materials and Methods; 95% confidence intervals estimated using Monte Carlo analyses are given in brackets.

mechanism that is capable of describing the major features of the data, while judiciously ignoring the possibility that there are more than two configurations of partially bound TRAP 11-mer rings. Although this BB model is clearly a simplification, the fitted kinetic parameters and their temperature dependencies nevertheless provide bulk kinetic and thermodynamic insights into the pathway of ligand binding and activation of TRAP.

Binding of Trp to TRAP Is Positively Cooperative. TRAP functions through heterotropic allostery, as binding of RNA to TRAP and binding of Trp to TRAP are strongly coupled.[37] Given the oligomeric structure of TRAP, its ligand-coupled disorder−order transition, and the geometric proximity of its ligand-binding sites to one another, the question of its homotropic allostery, or cooperativity in Trp binding, has long been of interest.[38−40] Efforts to investigate this question using equilibrium dialysis and calorimetry have revealed weak positive cooperativity for *B. subtilis* TRAP,[38] but not for *Bst* TRAP.[11,18,41,42] Our results clearly establish positive cooperativity in binding of Trp to *Bst* TRAP and provide a plausible mechanistic explanation for the phenomenon: initial weak binding by a fractional set of Trp ligands is followed by concerted structural changes that kinetically allow binding of additional Trp ligands, after which dissociation of the ligands is kinetically disfavored; we note also that the similar enthalpy changes for the two binding modes would complicate their detection by ITC as in refs 11 and 18 (Table 1). Although the BB kinetic model does not explicitly include a kinetic step for conformational change, the fact that all of the Trp-binding sites in the ring are structurally equivalent because of its axial symmetry requires that structural changes in the protein ring define the difference between binding modes that allow fast and slow ligand release. The nature of these structural changes is evident from the temperature dependence of the kinetic parameters, as described below.

The Temperature Dependence of Stopped-Flow Data Describes the Structural Differences between the Ground States Sampled by TRAP and between Their Intermediates. The observed large reduction in heat capacity upon Trp binding [$\Delta C_p \sim -506 + -1048 = -1554$ cal mol^{-1} K^{-1} (Table 3)] is much larger than that obtained from equilibrium calorimetric studies of wild-type TRAP (−370 cal mol^{-1} K^{-1};[11] this difference in ΔC_p is perhaps due to different protein sequences and experimental observables and perhaps the fact that the value of −370 cal mol^{-1} K^{-1} was obtained under conditions where the energetics of each Trp binding event was not evident[32,42,43]). If a reduction in C_p is considered a metric for the conformational restriction and/or compression of TRAP, these results imply that (i) the T + W free state is relatively loosely packed, (ii) the first Trp binding rapidly compresses TRAP through the transition state to the singly bound ground state, and (iii) the singly bound state is compressed even further upon the second binding to the doubly bound ground state (Figure 6). After solvation effects have been accounted for, this large negative ΔC_p implies a dramatic conformational restriction,[35] which is mechanistically consistent with NMR studies that detail conformational restriction on the microsecond to millisecond time scale upon Trp binding.[1,10]

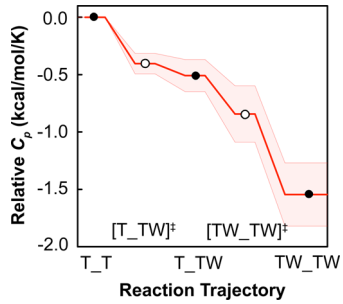

Figure 6. Extended Arrhenius analysis reveals a stepwise structural compression of TRAP upon Trp binding, evidenced by a reduction in heat capacity, C_p, along the reaction coordinate. The relative heat capacity along the reaction coordinate results from changes in structure and dynamics among the three ground states marked with black circles (T_T, T_TW, and TW_TW) via the two transition states marked with white circles ([T_TW]‡ and [TW_TW]‡). A lower value of C_p is interpreted as a conformational restriction of the Trp−TRAP−solvent system that releases otherwise-bound solvent molecules. The C_p of the T_T state is set to zero for reference, and the shaded region encloses propagated fitting errors via the extended Arrhenius relation. The largest changes in C_p occur between the ground state of free protein T_T and first transition state [T_TW]‡, and between second transition state [TW_TW]‡ and the fully bound state.

The Kinetics and Thermodynamics of TRAP Isomerization Influence Function. The rate constant for binding of Trp to TRAP, k_1^F, is small compared to that of other proteins that bind similarly shaped ligands (i.e., 0.65 μM^{-1} s^{-1} at 30 °C vs 1−1000 μM^{-1} s^{-1} for other proteins[44]). For example, Trp binds to TRAP 6−100 times slower than it does to the *trp* repressor: NMR line shape analyses yielded a value of 4.4 μM^{-1} s^{-1} at 30 °C,[45] while stopped-flow fluorescence experiments with the *trp* repressor yielded a rate constant of 4 μM^{-1} s^{-1} at 4 °C;[46] at that temperature, the Arrhenius analysis performed here predicts a value of 0.066 μM^{-1} s^{-1} for TRAP. These kinetic differences highlight differences in the Trp binding modes as, for instance, Trp binds to the surface of each protomer in the *trp* repressor dimer, where it remains solvent-accessible,[47] whereas Trp is buried between protomers in the TRAP 11-mer, where it is excluded from solvent.[13] It is clear that Trp binding is orders of magnitude slower than hydrodynamic estimates of the diffusion limit for such

encounters, even after considering uncertainties in the calculated encounter probability arising from estimates of the Trp binding area, and the diffusive encounter rate. Although low binding probability is not uncommon in other proteins,[48,49] solution NMR studies have shown apo TRAP to be quite dynamic at the Trp site.[1,10] This observation suggests that the flexible loops flanking the Trp-binding site function as a dynamic gate, directly influencing the mechanism and rate of Trp entry and solvent exit.[50−52]

In addition to modulating binding of Trp to apo TRAP, protein dynamics are important for allowing Trp release and deactivation. Because Trp is entirely buried in its fully bound state, release of bound Trp implies flexibility of holo TRAP on the time scale of the release rate constant for the second bound state, k_2^B, which ranges from 0.01 to 0.88 s^{-1} between 15 and 45 °C. Motions at these relatively slow time scales ($1/k$ = 1.1−100 s) are consistent with the observation that Ile 26δ_1 in the Trp loop samples two conformations in holo TRAP,[1] though we note that Trp fluorescence likely only reports on the dynamics of the binding pocket.[c] The fact that Trp release is slow relative to the time scale of bond rotations may reflect the requirement for a rare synchrony of individual local motions that occur at faster time scales (e.g., involving multiple residues or multiple protomers).[8] Indeed, such microsecond to millisecond motions have been observed near the RNA site and the core of holo TRAP, albeit to a small degree,[1] and indicate that the dynamic landscape of holo TRAP is surprisingly rich.

Key Insights and Limitations. Technical limitations arise in the interpretation of the physical observable in the stopped-flow data, Trp quantum yield Φ_{Trp}, because it is a one-dimensional value that is influenced by complex multidimensional effects from protein structure and dynamics.[33] In the BB model applied here, the change in Φ_{Trp} that reports on the first and second steps is interpreted as reporting Trp binding in a manner independent of configuration or nearest-neighbor effects, but there also may be changes in Φ_{Trp} associated with a conformational change in TRAP surrounding bound Trp and/or a reorganization of Trp molecules within a TRAP 11-mer. Furthermore, Φ_{Trp} may change depending on the number of Trp molecules bound to a single TRAP 11-mer, but this change could not be quantitatively defined in models that describe conformational changes between binding events (e.g., model E [BIB] in the Supporting Information).

Moreover, although the BB model appears to be adequate for broadly describing the kinetics of binding of Trp to TRAP, it is limited in its description of the 11 unique Trp-binding sites on each TRAP ring. Considering the oligomeric nature of TRAP, the mechanism of the BB model implies two assumptions. (i) There are only two types of binding events in the 11-mer, implying that binding sites with one occupied neighbor are similar to those with two occupied neighbors,[17] and (ii) each phase of the SF time course is exclusively binding. Thus, the BB model does not allow for a quantitative description of microscopic conformational changes in TRAP and/or a reorganization of Trp molecules within a TRAP 11-mer (i.e., Trp may be released from a kinetically favored site and rebound to a thermodynamically favored site). Despite these limitations, as discussed above, the BB model represents a prudent simplification because more complex models cannot be quantitatively constrained by these data.

CONCLUSION

The functions of proteins are dependent on their structure and dynamics, which are characterized by a conformational landscape that is sensitive to a variety of factors, including ligand binding, temperature, and pH.[8] Here, we shed light on these phenomena by characterizing the pathway through which the protein TRAP is activated by the ligand Trp (Figure 7).

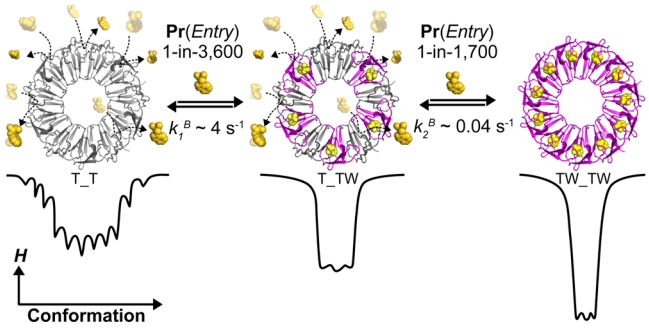

Figure 7. Bind−bind (BB) kinetic model for binding of Trp to TRAP. The BB model might be understood structurally by considering binding of the first set of Trp molecules to sites without occupied neighboring sites, while the second set of Trp ligands binds after partial ring saturation has resulted in stabilization of a higher-affinity binding mode; the figure illustrates one such possible intermediate. Quantitatively, the results of the BB analysis reveal that in the free state (T_T), TRAP is conformationally diverse and Trp binding requires ~3600 encounters before successful entry. Once the first Trp molecule binds, the Trp-binding site undergoes a rapid conformational restriction (i.e., reduction in C_p) in which initial Trp bonds are formed. Moreover, after the first Trp binding, the neighboring Trp sites may be structurally and/or dynamically altered such that the second Trp binding is ~50% faster and ~150 times tighter than the first Trp binding. The binding probabilities and rate constants correspond to data at 25 °C.

Prior studies have indicated that the flexibility of apo TRAP is important for the prevention of RNA binding.[1,10] Here, we have expanded this view by showing that the flexibility of apo TRAP may play a role in gating the entry of Trp, shown here to involve more than 6000 unsuccessful attempts at some temperatures, as a possible mechanism for enhanced ligand selectivity.[51,52] Moreover, the flexibility of apo TRAP may help characterize the extent to which any allosteric effects in TRAP involve induced fit or conformational selection mechanisms.[49,50,53] Next, a two-binding site kinetic model reveals the mechanism of positive homotropic cooperativity for Trp binding: weak binding by an initial set of Trp ligands is followed by a change in the structure and dynamics of TRAP that permits a higher-affinity binding mode, from which Trp release is retarded by 100-fold. Next, although structural and thermodynamic studies have already indicated that holo TRAP is more bonded, more ordered, and more conformationally restricted than apo TRAP,[11] our present kinetic data reveal that these interactions proceed in a stepwise manner through intermediate states. Finally, despite the relative rigidity of holo TRAP,[1,10] because the release of Trp from doubly bound TRAP occurs on the subsecond time scale between two bound states, we conclude that the flexibility of holo TRAP on this time scale may be important for bound Trp to exit its otherwise buried binding site. Finally, considering that holo TRAP also exhibits flexibility on the microsecond to millisecond time scale,[1,10] our results reveal that holo TRAP exhibits a rich dynamic behavior

dx.doi.org/10.1021/bi401364v | Biochemistry 2013, 52, 8855−8865

that illustrates how changes in the conformational landscape coincide with molecular function.

■ ASSOCIATED CONTENT

Supporting Information

Details of the model selection process and stopped-flow data and fits at all seven temperatures. This material is available free of charge via the Internet at http://pubs.acs.org.

■ AUTHOR INFORMATION

Corresponding Author

*Address: 484 W. 12th Ave., Columbus, OH 43210. E-mail: foster.281@osu.edu. Phone: (614) 292-1377. Fax: (614) 292-6773.

Funding

This project was funded by National Institutes of Health Grants GM077234, GM65183, and GM067153 and National Science Foundation Grant MCB 1019960.

Notes

The authors declare no competing financial interest.

■ ACKNOWLEDGMENTS

We thank Brandon Stilb (University at Buffalo, the State University of New York) for assistance with sample preparation, Richard Swenson (The Ohio State University) for stopped-flow training and advice during preliminary experiments, Zucai Suo, Amy Xu (The Ohio State University), Michael Ibba, and Samhita Yadavalli (The Ohio State University) for their help in conducting the stopped-flow experiments. In addition, we thank Petr Huan-Xiang Zhou (Florida State University, Tallahassee, FL) for input regarding Trp orientation and Amber Simmons for careful review of the manuscript.

■ ABBREVIATIONS

TRAP, *trp* RNA-binding attenuation protein; Trp and W, tryptophan; NMR, nuclear magnetic resonance; SF, stopped-flow; Φ, quantum yield; k, rate constant; K, equilibrium constant; G, Gibbs free energy; H, enthalpy; S, entropy; C_p, heat capacity; ΔX, change in quantity X (X = G, H, S, or C_p); $X^{\ddagger}$, transition state quantity X.

■ ADDITIONAL NOTES

[a]In this work, TRAP refers to the A26I variant of *B. stearothermophilus* (*Bst*) TRAP, which displays RNA binding and tryptophan binding characteristics similar to those of the wild-type protein, and was used to make direct comparisons with related NMR studies.[1]

[b]We also formulated a TRAP 11-mer version of allosteric models used in other systems, such as the two-state Monod−Wyman−Changeux model for hemoglobin,[2] the tertiary two-state model for hemoglobin,[3] comparative Markov models for tetrameric ion channels,[4,5] and conformational spread in a ring of proteins.[6,7] Considering that mechanisms describing three binding steps were too complex to yield informative fits, it is not surprising that these more complex 11-mer models were also too complex to yield informative fits.

[c]Even though Trp probes a local region of structure, the thermodynamic quantities G, H, S, and C_p reflect the entire protein−ligand−solvent system.

■ REFERENCES

(1) Kleckner, I. R., Gollnick, P., and Foster, M. P. (2012) Mechanisms of allosteric gene regulation by NMR quantification of μs-ms protein dynamics. *J. Mol. Biol. 415*, 372−381.

(2) Henry, E. R., Jones, C. M., Hofrichter, J., and Eaton, W. A. (1997) Can a two-state MWC allosteric model explain hemoglobin kinetics? *Biochemistry 36*, 6511−6528.

(3) Henry, E. R., Bettati, S., Hofrichter, J., and Eaton, W. A. (2002) A tertiary two-state allosteric model for hemoglobin. *Biophys. Chem. 98*, 149−164.

(4) Nekouzadeh, A., Silva, J. R., and Rudy, Y. (2008) Modeling subunit cooperativity in opening of tetrameric ion channels. *Biophys. J. 95*, 3510−3520.

(5) Zagotta, W. N., Hoshi, T., and Aldrich, R. W. (1994) Shaker potassium channel gating. III: Evaluation of kinetic models for activation. *J. Gen. Physiol. 103*, 321−362.

(6) Bai, F., Branch, R. W., Nicolau, D. V. J., Pilizota, T., Steel, B. C., Maini, P. K., and Berry, R. M. (2010) Conformational spread as a mechanism for cooperativity in the bacterial flagellar switch. *Science 327*, 685−689.

(7) Duke, T. A., Le Novère, N., and Bray, D. (2001) Conformational spread in a ring of proteins: A stochastic approach to allostery. *J. Mol. Biol. 308*, 541−553.

(8) Henzler-Wildman, K., and Kern, D. (2007) Dynamic personalities of proteins. *Nature 450*, 964−972.

(9) Gollnick, P., Babitzke, P., Antson, A., and Yanofsky, C. (2005) Complexity in regulation of tryptophan biosynthesis in *Bacillus subtilis*. *Annu. Rev. Genet. 39*, 47−68.

(10) McElroy, C., Manfredo, A., Wendt, A., Gollnick, P., and Foster, M. (2002) TROSY-NMR studies of the 91 kDa TRAP protein reveal allosteric control of a gene regulatory protein by ligand-altered flexibility. *J. Mol. Biol. 323*, 463−473.

(11) McElroy, C. A., Manfredo, A., Gollnick, P., and Foster, M. P. (2006) Thermodynamics of tryptophan-mediated activation of the trp RNA-binding attenuation protein. *Biochemistry 45*, 7844−7853.

(12) Malay, A. D., Watanabe, M., Heddle, J. G., and Tame, J. R. H. (2011) Crystal structure of unliganded TRAP: Implications for dynamic allostery. *Biochem. J. 434*, 427−434.

(13) Antson, A. A., Otridge, J., Brzozowski, A. M., Dodson, E. J., Dodson, G. G., Wilson, K. S., Smith, T. M., Yang, M., Kurecki, T., and Gollnick, P. (1995) The structure of trp RNA-binding attenuation protein. *Nature 374*, 693−700.

(14) Chen, X. P., Antson, A. A., Yang, M., Li, P., Baumann, C., Dodson, E. J., Dodson, G. G., and Gollnick, P. (1999) Regulatory features of the trp operon and the crystal structure of the trp RNA-binding attenuation protein from *Bacillus stearothermophilus*. *J. Mol. Biol. 289*, 1003−1016.

(15) Antson, A. A., Dodson, E. J., Dodson, G., Greaves, R. B., Chen, X., and Gollnick, P. (1999) Structure of the trp RNA-binding attenuation protein, trap, bound to RNA. *Nature 401*, 235−242.

(16) Watanabe, M., Heddle, J. G., Kikuchi, K., Unzai, S., Akashi, S., Park, S., and Tame, J. R. H. (2009) The nature of the TRAP-anti-TRAP complex. *Proc. Natl. Acad. Sci. U.S.A. 106*, 2176−2181.

(17) Saroff, H. A., and Kiefer, J. E. (1997) Analysis of the binding of ligands to large numbers of sites: The binding of tryptophan to the 11 sites of the trp RNA-binding attenuation protein. *Anal. Biochem. 247*, 138−142.

(18) Heddle, J. G., Okajima, T., Scott, D. J., Akashi, S., Park, S., and Tame, J. R. H. (2007) Dynamic allostery in the ring protein TRAP. *J. Mol. Biol. 371*, 154−167.

(19) Wilkins, M. R., Gasteiger, E., Bairoch, A., Sanchez, J. C., Williams, K. L., Appel, R. D., and Hochstrasser, D. F. (1999) Protein identification and analysis tools in the expasy server. *Methods Mol. Biol. 112*, 531−552.

(20) Fasman, G. (1976) *Handbook of biochemistry and molecular biology, proteins*, 3rd ed., CRC Press, Boca Raton, FL.

(21) Kuzmic, P. (1996) Program dynafit for the analysis of enzyme kinetic data: Application to HIV proteinase. *Anal. Biochem. 237*, 260−273.

(22) Kuzmic, P. (2009) Dynafit: A software package for enzymology. *Methods Enzymol. 467*, 247−280.
(23) Cantor, C. R., and Schimmel, P. R. (1980) *Biophysical Chemistry: Part III: The Behavior of Biological Macromolecules*, 1st ed., W. H. Freeman, New York.
(24) Motulsky, H. J., and Christopoulos, A. (2003) *Fitting Models to Biological Data Using Linear and Nonlinear Regression. A Practical Guide to Curve Fitting*, 2nd ed., Graphpad Software Inc., San Diego.
(25) Shoup, D., Lipari, G., and Szabo, A. (1981) Diffusion-controlled bimolecular reaction rates. The effect of rotational diffusion and orientation constraints. *Biophys. J. 36*, 697−714.
(26) Smoluchowski, M. (1915) Über brownsche molekularbewegung unter einwirkung äußerer kräfte und den zusammenhang mit der verallgemeinerten diffusionsgleichung. *Ann. Phys. 48*, 1103−1112.
(27) Lide, D. R., Ed. (2014) *CRC Handbook of Chemistry and Physics*, 94th ed., Taylor and Francis, New York.
(28) Solc, K., and Stockmayer, W. H. (1973) Kinetics of diffusion-controlled reaction bewteen chemically asymmetric molecules. II. Approximate steady-state solution. *Int. J. Chem. Kinet. 5*, 733−752.
(29) Winzor, D. J., and Jackson, C. M. (2006) Interpretation of the temperature dependence of equilibrium and rate constants. *J. Mol. Recognit. 19*, 389−407.
(30) Goldberg, J. M., and Baldwin, R. L. (1998) Kinetic mechanism of a partial folding reaction. 2. Nature of the transition state. *Biochemistry 37*, 2556−2563.
(31) Keleti, T. (1983) Errors in the evaluation of Arrhenius and van't Hoff plots. *Biochem. J. 209*, 277−280.
(32) Naghibi, H., Tamura, A., and Sturtevant, J. M. (1995) Significant discrepancies between van't Hoff and calorimetric enthalpies. *Proc. Natl. Acad. Sci. U.S.A. 92*, 5597−5599.
(33) Lakowicz, J. R. (2006) *Principles of Fluorescence Spectroscopy*, 3rd ed., Springer, New York.
(34) Goldberg, J. M., and Baldwin, R. L. (1998) Kinetic mechanism of a partial folding reaction. 1. Properties of the reaction and effects of denaturants. *Biochemistry 37*, 2546−2555.
(35) Prabhu, N. V., and Sharp, K. A. (2005) Heat capacity in proteins. *Annu. Rev. Phys. Chem. 56*, 521−548.
(36) Barbolina, M. V., Kristoforov, R., Manfredo, A., Chen, Y., and Gollnick, P. (2007) The rate of trap binding to RNA is crucial for transcription attenuation control of the *B. subtilis* trp operon. *J. Mol. Biol. 370*, 925−938.
(37) Babitzke, P., and Yanofsky, C. (1995) Structural features of L-tryptophan required for activation of TRAP, the trp RNA-binding attenuation protein of *Bacillus subtilis*. *J. Biol. Chem. 270*, 12452−12456.
(38) Antson, A. A., Otridge, J., Brzozowski, A. M., Dodson, E. J., Dodson, G. G., Wilson, K. S., Smith, T. M., Yang, M., Kurecki, T., and Gollnick, P. (1995) The structure of trp RNA-binding attenuation protein. *Nature 374*, 693−700.
(39) Yang, M., Chen, X. P., Militello, K., Hoffman, R., Fernandez, B., Baumann, C., and Gollnick, P. (1997) Alanine-scanning mutagenesis of *Bacillus subtilis* trp RNA-binding attenuation protein (TRAP) reveals residues involved in tryptophan binding and RNA binding. *J. Mol. Biol. 270*, 696−710.
(40) Li, P. T. X., Scott, D. J., and Gollnick, P. (2002) Creating hetero-11-mers composed of wild-type and mutant subunits to study RNA binding to TRAP. *J. Biol. Chem. 277*, 11838−11844.
(41) Chen, X. P., Antson, A. A., Yang, M., Li, P., Baumann, C., Dodson, E. J., Dodson, G. G., and Gollnick, P. (1999) Regulatory features of the trp operon and the crystal structure of the trp RNA-binding attenuation protein from *Bacillus stearothermophilus*. *J. Mol. Biol. 289*, 1003−1016.
(42) Mizoue, L. S., and Tellinghuisen, J. (2004) Calorimetric vs. van't hoff binding enthalpies from isothermal titration calorimetry: Ba^{2+}-crown ether complexation. *Biophys. Chem. 110*, 15−24.
(43) Horn, J. R., Russell, D., Lewis, E. A., and Murphy, K. P. (2001) van't Hoff and calorimetric enthalpies from isothermal titration calorimetry: Are there significant discrepancies? *Biochemistry 40*, 1774−1778.
(44) Hammes, G., and Schimmel, P. (1970) in *The Enzymes* (Boyer, P., Ed.) 1st ed., Academic Press, New York.
(45) Schmitt, T. H., Zheng, Z., and Jardetzky, O. (1995) Dynamics of tryptophan binding to *Escherichia coli* trp repressor wild type and av77 mutant: An NMR study. *Biochemistry 34*, 13183−13189.
(46) Chou, W. Y., Bieber, C., and Matthews, K. S. (1989) Tryptophan and 8-anilino-1-naphthalenesulfonate compete for binding to trp repressor. *J. Biol. Chem. 264*, 18309−18313.
(47) Schevitz, R. W., Otwinowski, Z., Joachimiak, A., Lawson, C. L., and Sigler, P. B. (1985) The three-dimensional structure of trp repressor. *Nature 317*, 782−786.
(48) Cai, L., and Zhou, H. (2011) Theory and simulation on the kinetics of protein-ligand binding coupled to conformational change. *J. Chem. Phys. 134*, 105101.
(49) Sullivan, S. M., and Holyoak, T. (2008) Enzymes with lid-gated active sites must operate by an induced fit mechanism instead of conformational selection. *Proc. Natl. Acad. Sci. U.S.A. 105*, 13829−13834.
(50) Kempner, E. S. (1993) Movable lobes and flexible loops in proteins. Structural deformations that control biochemical activity. *FEBS Lett. 326*, 4−10.
(51) Zhou, H., and McCammon, J. A. (2010) The gates of ion channels and enzymes. *Trends Biochem. Sci. 35*, 179−185.
(52) Zhou, H. X., Wlodek, S. T., and McCammon, J. A. (1998) Conformation gating as a mechanism for enzyme specificity. *Proc. Natl. Acad. Sci. U.S.A. 95*, 9280−9283.
(53) Zhou, H. (2010) From induced fit to conformational selection: A continuum of binding mechanism controlled by the timescale of conformational transitions. *Biophys. J. 98*, L15−L17.

Supporting Information

Homotropic Cooperativity from the Activation Pathway of the Allosteric Ligand-Responsive Regulatory Protein TRAP†

Ian R. Kleckner[a], Craig A. McElroy[b], Petr Kuzmic[c],Paul Gollnick[d], Mark P. Foster[a,b]*

[a]Biophysics Program, The Ohio State University, 484 West 12th Ave, Columbus, OH 43210

[b] Departments of Chemistry and Biochemistry, and Center for RNA Biology, The Ohio State University, 484 West 12th Ave, Columbus, OH 43210

[c]BioKin Ltd., 15 Main Street Suite 232, Watertown, MA 02472

[d] Department of Biological Sciences, University at Buffalo, the State University of New York, Buffalo, NY 14260

email contacts: ian.kleckner@gmail.com, mcelroy.31@gmail.com, pkuzmic2@biokin.com, gollnick@buffalo.edu, foster.281@osu.edu

† This project was funded by the National Institutes of Health grant R01GM077234, and grant # 1019960 from the National Science Foundation.

* Corresponding author: 484 West 12th Ave, Columbus, OH, 43210, USA. Phone: (614) 292-1377; Fax: (614) 292-6773; Foster.281@osu.edu

Supporting Information

Testing and discriminating candidate models. The program DYNAFIT version 4 (1, 2) was used to compare a variety of models to fit the stopped-flow (SF) data because it permits numerical integration of the rate laws that it automatically derives from an arbitrary reaction mechanism, thus simplifying the comparison process. Ten two- and three-step mechanisms involving binding of Trp to TRAP with optional isomerization are listed below (models A through J). The abbreviations used are [B] = binding, [I] = isomerization, W = Trp, and T = TRAP. An isolated binding site is designated T, a pair of binding sites is designated T_T, and a triplet of binding sites is designated T_T_T. Each isomerization event is designated by an additional star (*) for the set of binding sites. For example, model A is "Bind-Bind [BB]" which describes a pair of binding sites (T_T) with two successive Trp binding steps with distinct binding rates k_1 and k_2. For clarity in the following figures, each rate k designates both forward and backward rate constants, k^F and k^B (i.e., the forward and backward rates are not shown explicitly, but they are used in the fitting process).

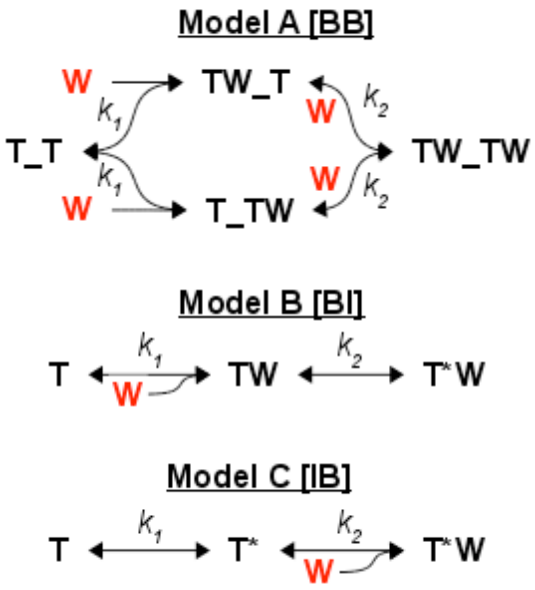

Model D [BBB]

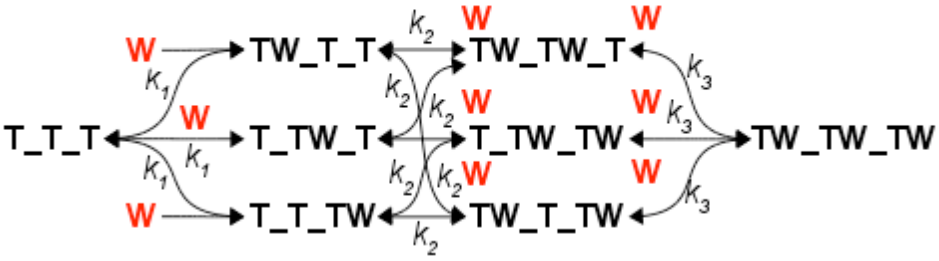

Model E [BIB]

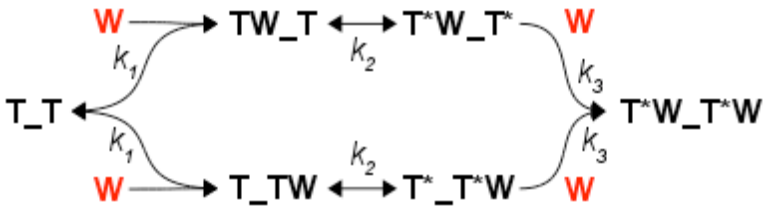

Model F [BBI]

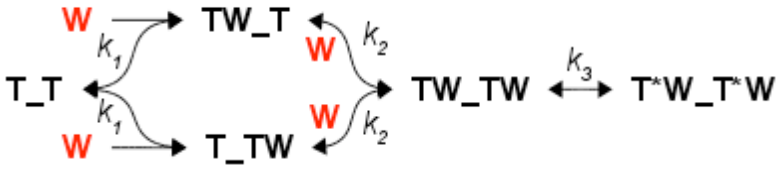

Model G [BII]

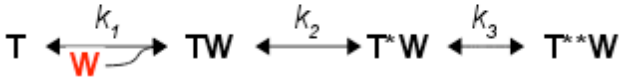

Model H [IBB]

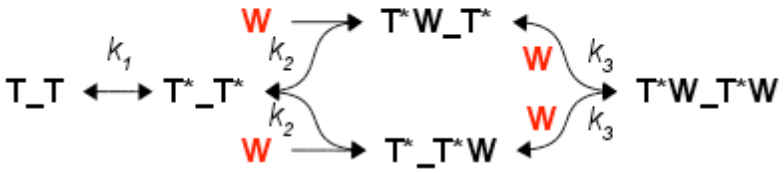

Model I [IIB]

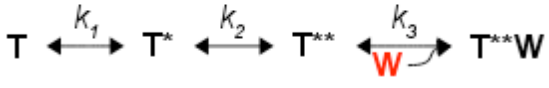

Model J [IBI]

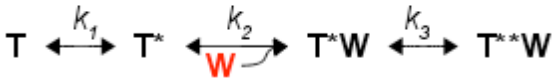

For each mechanism at each temperature, all the 6-7 SF time-courses acquired at that temperature were globally fit by specifying each of the post-mixing concentrations of Trp and TRAP that correspond to each time-course (n.b., the concentration of a pair of binding sites, T_T, is half the concentration of a single binding site, T). The fitted parameters were the forward and backwards rate constants for each kinetic step, k^F and k^B, the baseline offsets for each time-course, and one or more fluorescence response values, R, which were constrained as follows. States without Trp are considered invisible (i.e., $R = 0$). An isomerization event, designated here by adding a star (*) to the state, will change the response value (e.g., R(TW) and R(T*W) can differ). For the initial comparisons of the 10 models, fitting was made more tractable by assuming that a binding event scales the response value by the number of Trp molecules bound (e.g., R(TW_TW) = 2 * R(TW_T) = R(T_TW); otherwise there would be too many adjustable parameters in the model). Subsequent fits comparing the two most promising simpler models, A [BB] and B [BI], did not require this constraint because these models were simple enough to accommodate an extra fitting parameter (i.e., allowing R(TW_TW) to be indepent of R(TW_T)).

As discussed in the main text, model A [BB] appeared most appropriate to describe our data given the following model comparison procedure. First, comparisons of all ten models indicated that the three-step models (D, E, F, G, H, I, and J) were not appropriate because they always returned at least some parameter values that were not intelligible in some way, such as: (1) response values for some Trp-bound states were zero, which is physically unreasonable, (2) temperature-dependences of some parameters were physically unreasonable (e.g., sporadically changing with temperature, not

monotonically changing with temperature), or (3) fitting errors were over 1000% (i.e., undefined parameter value). The result that the three-step models were too complex is consistent with the multi-phase exponential fitting results, wherein although three-phase exponential models fit the data with smaller total residuals, the three-phase exponential model parameter values were poorly constrained (Fig. S1, Table S3). Next, we compared the three two step models (A, B, and C). Model A [BB] was statistically favored with the sum of squared errors (SSE) metric at all temperatures except for 45ºC, where models A [BB] and B [BI] were effectively equivalent (Table S1). Model C [IB] fit the data so poorly that it was obvious the mechanism was inappropriate.

Supporting Figures

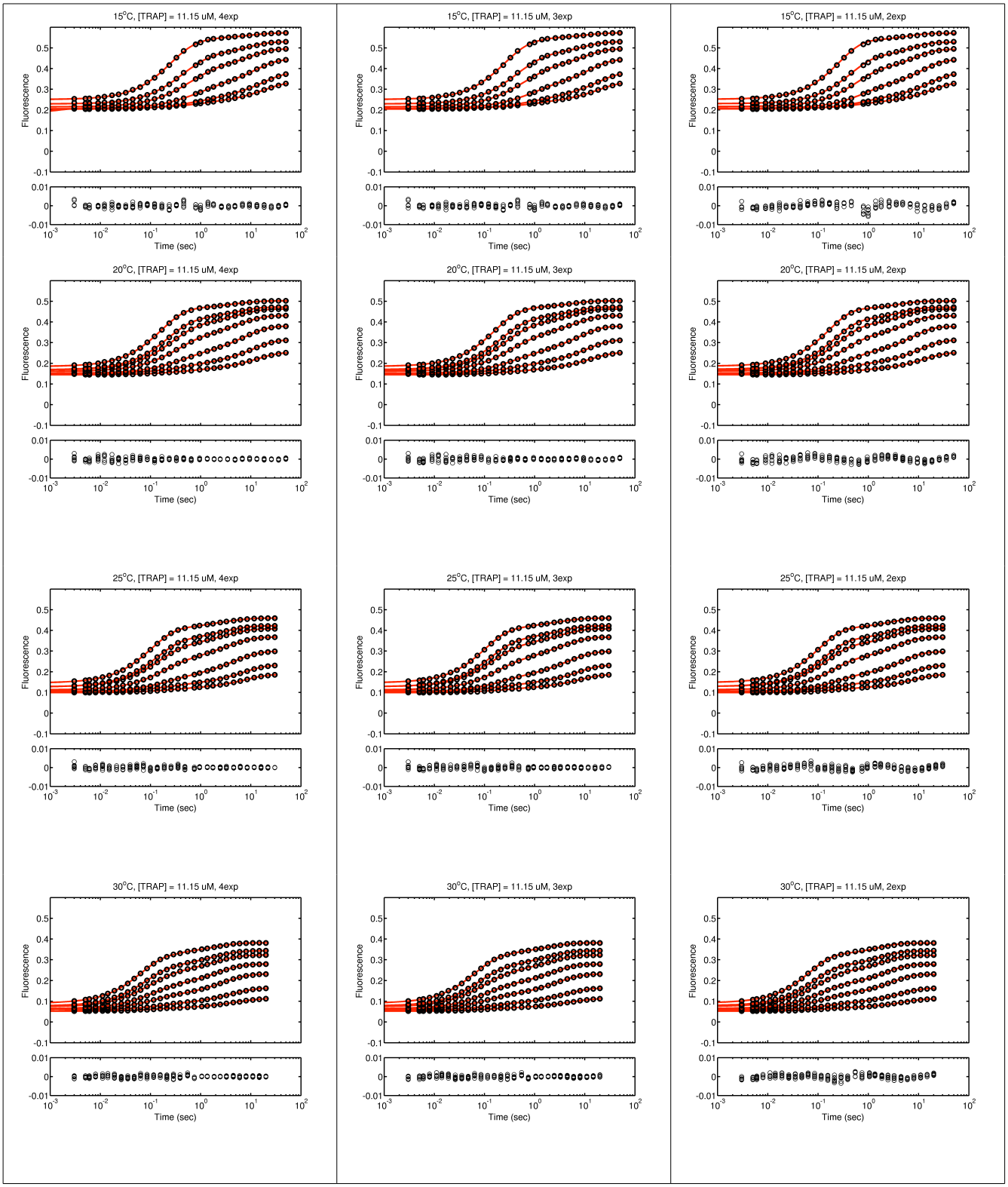

Figure S1 (continued)

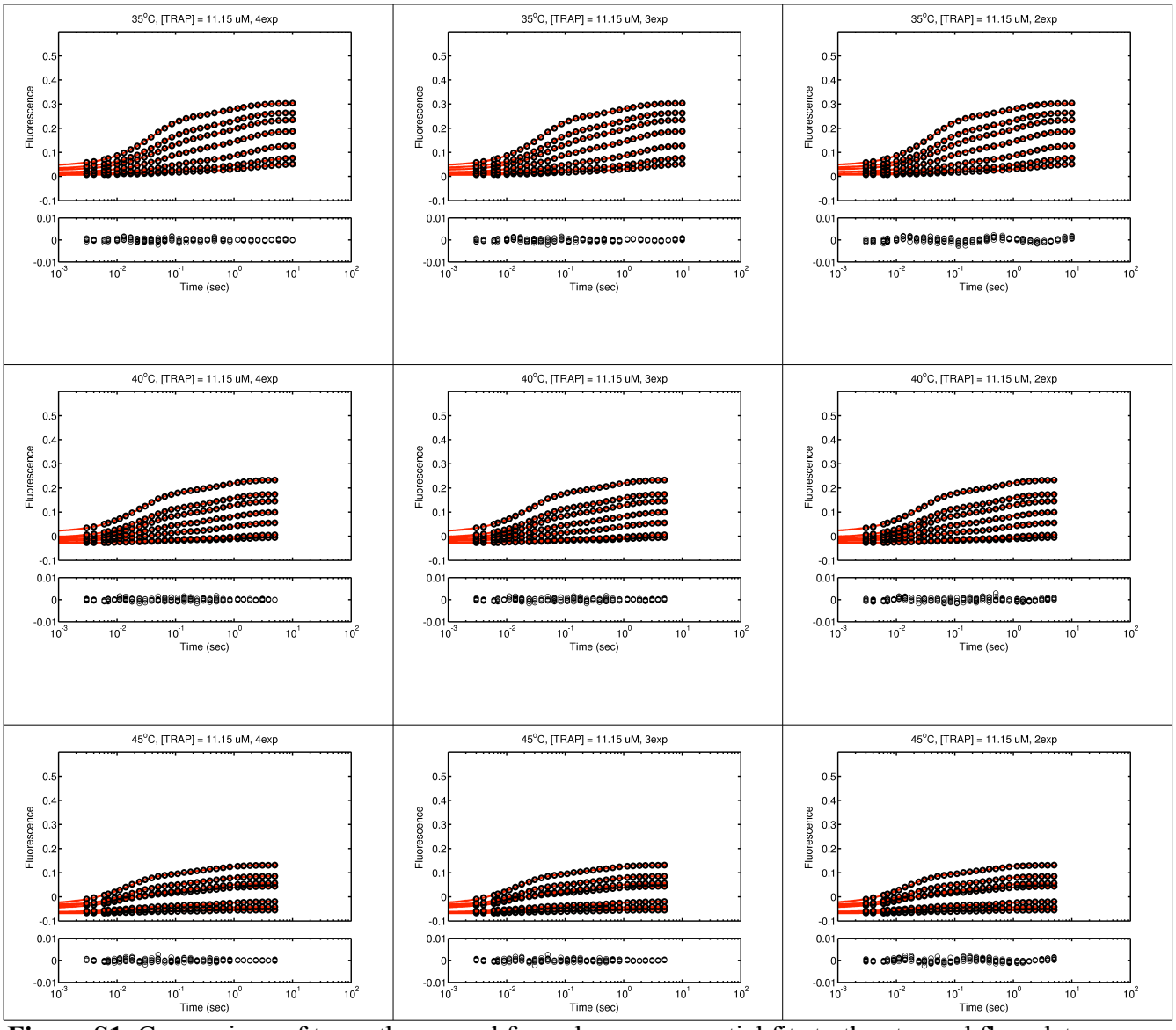

Figure S1. Comparison of two-, three-, and four-phase exponential fits to the stopped flow data. Three-phase exponential fits are generally preferred when fits are compared using the Bayesian Information Criterion (BIC; Table S3). However, the two-phase exponential fit does capture the two major phases of the time course (i.e., the initial fast phase and the final slow phase). The bottom of each panel shows the residuals, which are largest for the two-phase exponential fit.

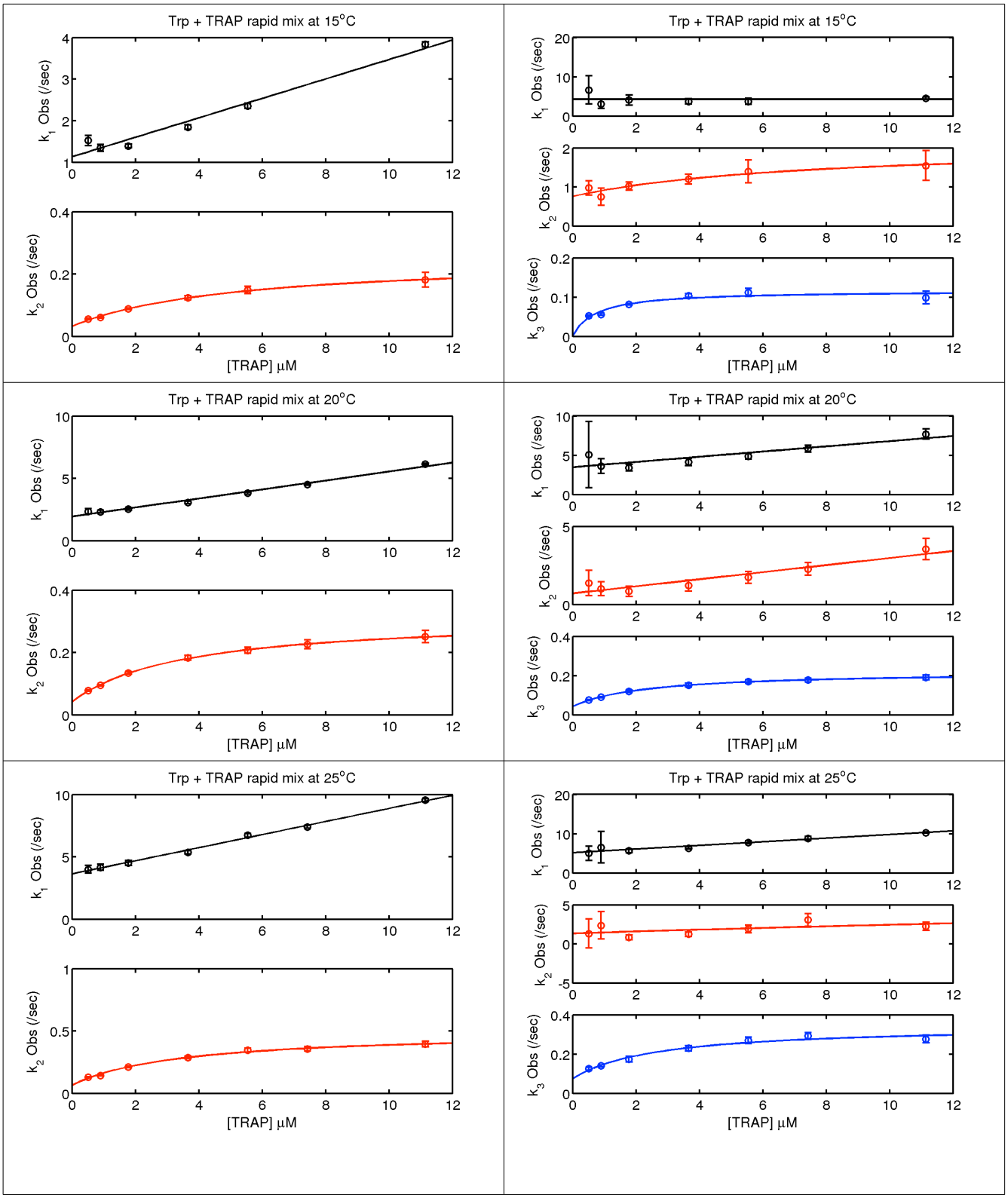
Trp + TRAP rapid mix at 15°C
k1 Obs (/sec)
k2 Obs (/sec)
[TRAP] µM
Trp + TRAP rapid mix at 15°C
k1 Obs (/sec)
k2 Obs (/sec)
k3 Obs (/sec)
[TRAP] µM
Trp + TRAP rapid mix at 20°C
k1 Obs (/sec)
k2 Obs (/sec)
[TRAP] µM
Trp + TRAP rapid mix at 20°C
k1 Obs (/sec)
k2 Obs (/sec)
k3 Obs (/sec)
[TRAP] µM
Trp + TRAP rapid mix at 25°C
k1 Obs (/sec)
k2 Obs (/sec)
[TRAP] µM
Trp + TRAP rapid mix at 25°C
k1 Obs (/sec)
k2 Obs (/sec)
k3 Obs (/sec)
[TRAP] µM

Figure S2 (continued)

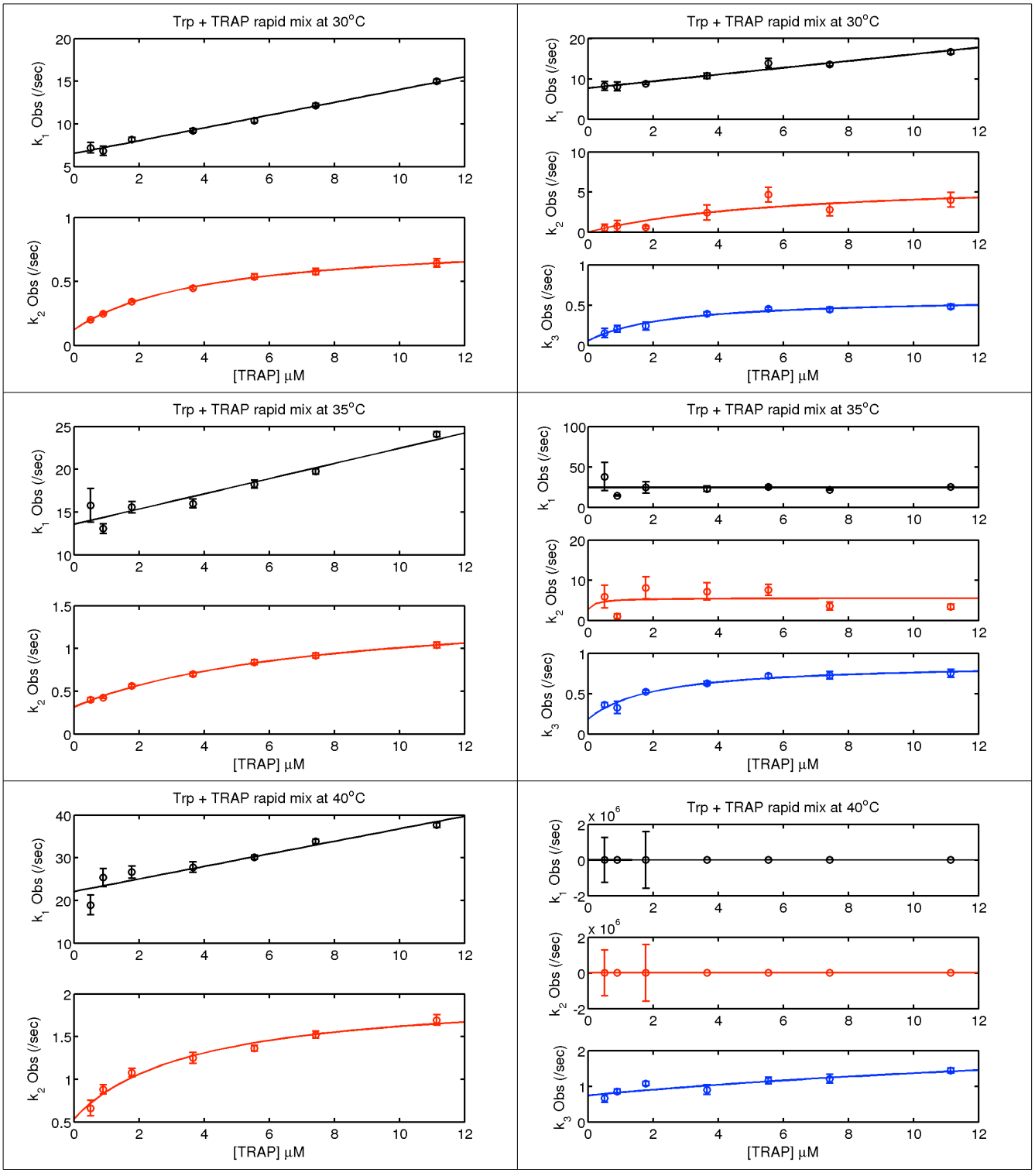

Figure S2 (continued)

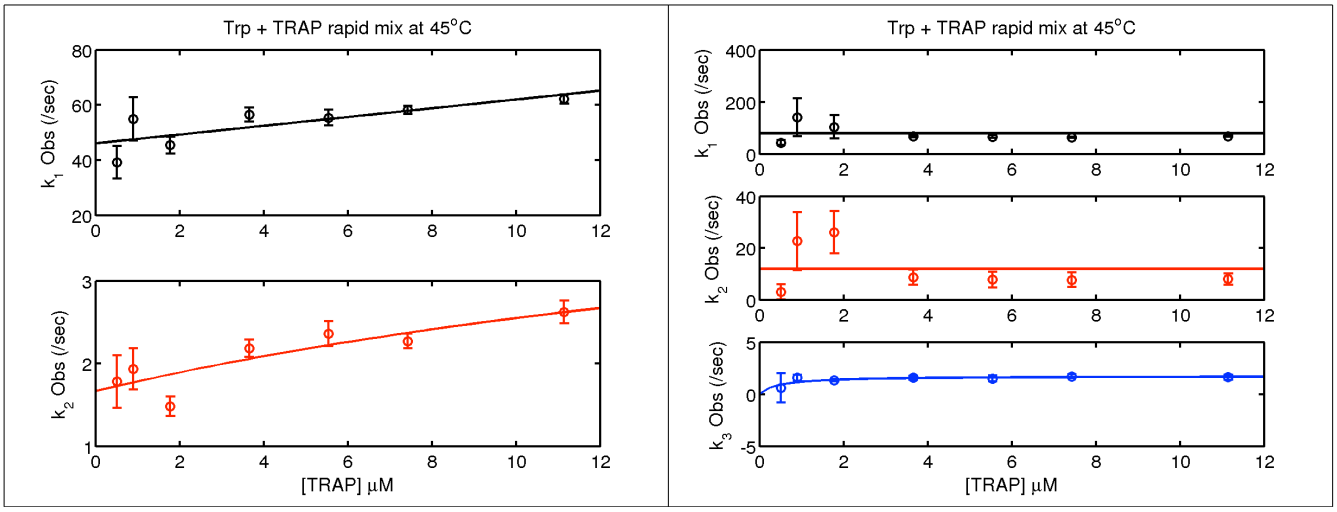

Figure S2. The concentration-dependence of the mechanism-independent apparent rate constants reveal that the second step mechanistically follows the first step. Each sub-figure shows one apparent rate constant obtained from the two- or three-phase exponential fit (left or right, respectively) plotted against the TRAP concentration in the sample where that rate constant was observed. The solid lines in each plot show fits of the k^{Obs} vs. [TRAP] to either a line or a hyperbola. For the two-phase exponential fits (left), the faster (first) step exhibits a linear relationship between k^{Obs} and [TRAP] and the second (slower) step exhibits a hyperbolic relationship between k^{Obs} and [TRAP]. For the three-phase exponential fits (right), there appears to be an additional step that occurs *between* steps 1 and 2 from the two-phase analysis (i.e., two-phase steps 1 and 2 are three-phase steps 1 and 3). Unfortunately, the three-phase exponential fit appears unintelligible as some rate constants are poorly defined (i.e., large error bars as in steps 1 and 2 at 40ºC), and as the data points do not lie near the theoretically expected fit lines. The error bars show the standard errors from fitting the time-dependent SF data to a two-phase or three-phase exponential function and are considered a lower-limit of the uncertainty. Fitted values are shown in Table S2.

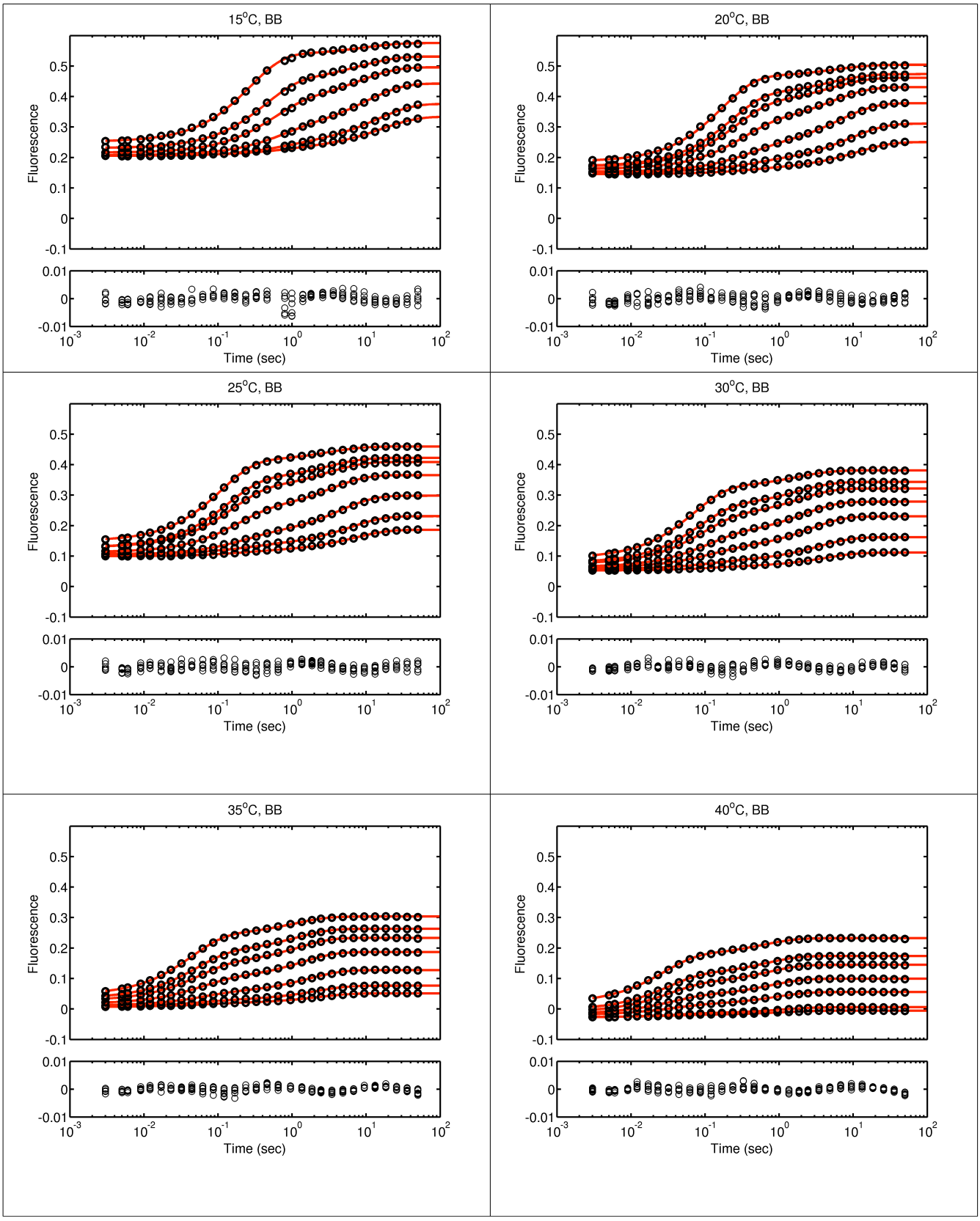
15°C, BB
20°C, BB
25°C, BB
30°C, BB
35°C, BB
40°C, BB
Fluorescence
Time (sec)

Figure S3 (continued)

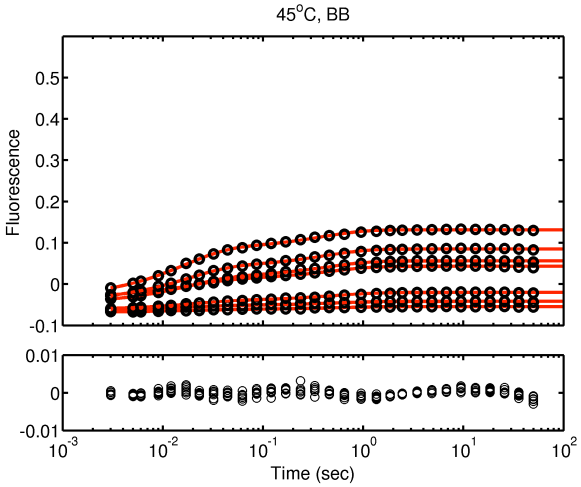

Figure S3. Stopped-flow data and fit to model A [BB] at each of seven temperatures (see above). Data at each of the seven time courses (A -G) correspond to 1 μM Trp mixed with TRAP 11-mer at concentrations of 0.093, 0.164, 0.323, 0.664, 1.008, 1.350, and 2.027 μM (1.022, 1.800, 3.558, 7.306, 11.088, 14.846, and 22.292 μM binding sites). Note, data at 15°C with 1.350 μM TRAP 11-mer were unreliable and were therefore removed.

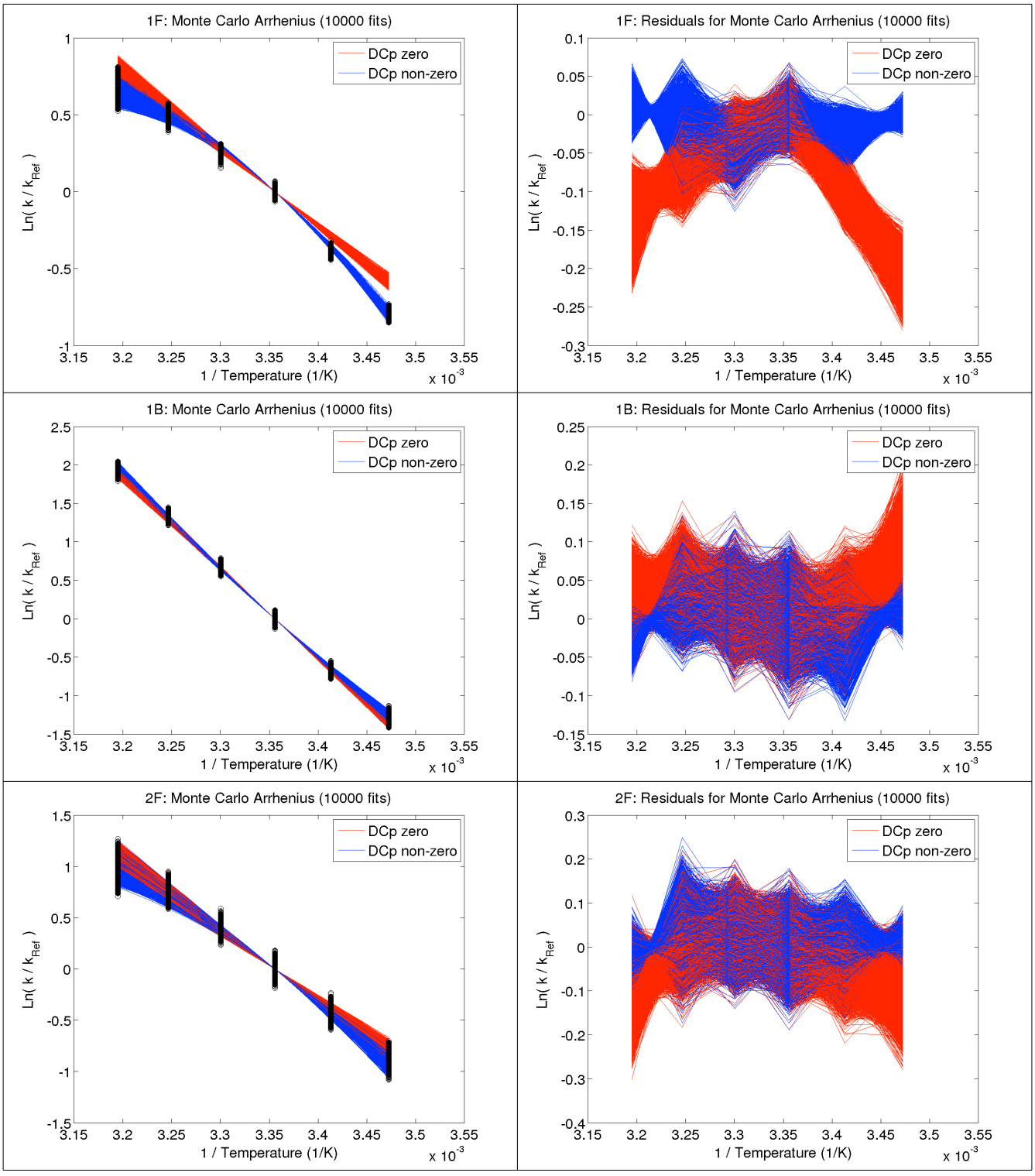
1F: Monte Carlo Arrhenius (10000 fits)
DCp zero
DCp non-zero
Ln(k / k_Ref)
1 / Temperature (1/K)
x 10^-3
1F: Residuals for Monte Carlo Arrhenius (10000 fits)
DCp zero
DCp non-zero
Ln(k / k_Ref)
1 / Temperature (1/K)
x 10^-3
1B: Monte Carlo Arrhenius (10000 fits)
DCp zero
DCp non-zero
Ln(k / k_Ref)
1 / Temperature (1/K)
x 10^-3
1B: Residuals for Monte Carlo Arrhenius (10000 fits)
DCp zero
DCp non-zero
Ln(k / k_Ref)
1 / Temperature (1/K)
x 10^-3
2F: Monte Carlo Arrhenius (10000 fits)
DCp zero
DCp non-zero
Ln(k / k_Ref)
1 / Temperature (1/K)
x 10^-3
2F: Residuals for Monte Carlo Arrhenius (10000 fits)
DCp zero
DCp non-zero
Ln(k / k_Ref)
1 / Temperature (1/K)
x 10^-3

Figure S4 (continued)

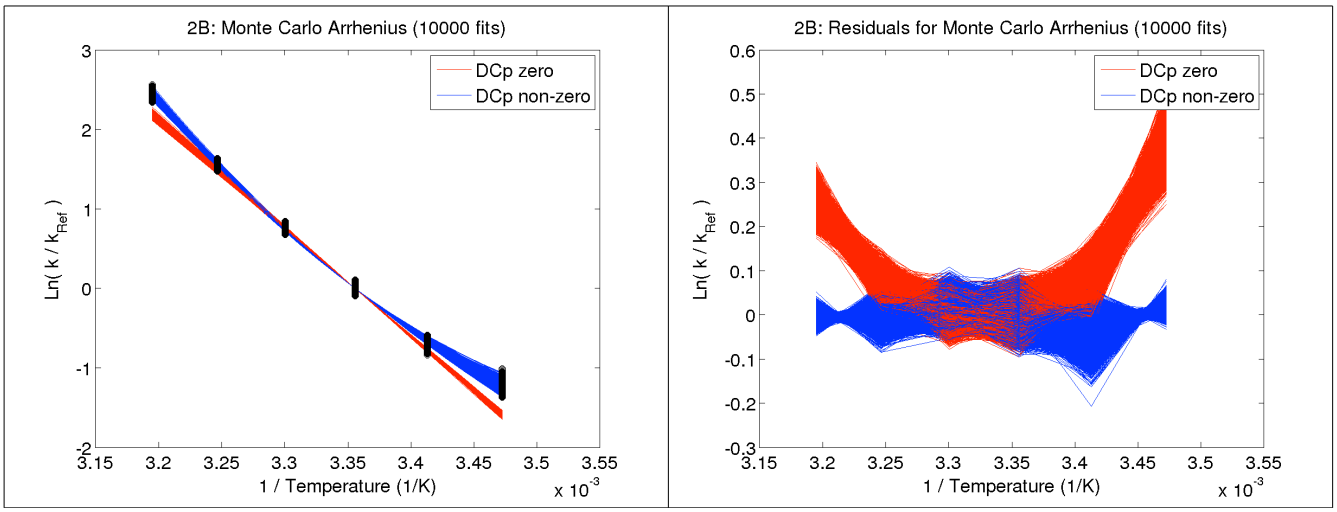

Figure S4. Arrhenius analyses of each of four kinetic rates extracted from the model A [BB] supports non-zero $\Delta C_p^{\ddagger}$ for steps 1F and 2B, whereas steps 1B and 2F are adequately described with zero $\Delta C_p^{\ddagger}$. However, we elected to use non-zero $\Delta C_p^{\ddagger}$ values for all four steps to retain consistency with both the principle of microscopic reversibility and with results from van't Hoff analysis (Fig S5). The Monte Carlo analysis produced two fits to each of 10,000 simulated datasets generated from re-sampling the distribution of residuals; the set of simulated datasets estimates the uncertainty in the measured values on the y-axis (i.e., $\ln(k_1^F / k_1^F{}_{Ref})$, etc.). The fit with $\Delta C_p^{\ddagger}$ set to zero (red line) produces a straight line with zero curvature, and yields curved residuals for steps 1F and 2B (right plots). This curvature is reduced when $\Delta C_p^{\ddagger}$ is non-zero (blue line), but the reduction in residuals is much more significant for steps 1F and 2B than for steps 1B and 2F.

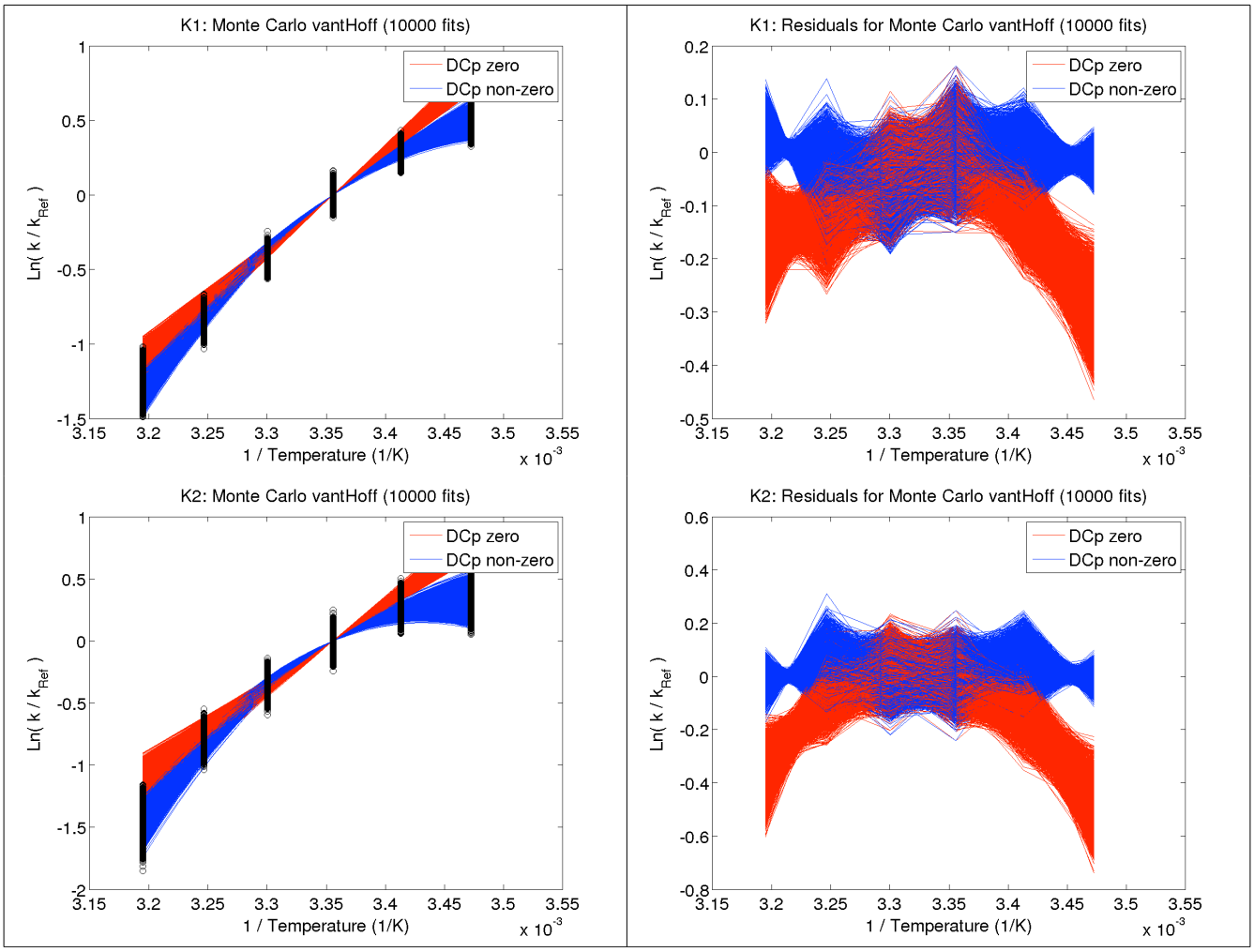

Figure S5. van't Hoff analyses of the two equilibrium constants extracted from the model A [BB] supports non-zero ΔC_p for steps 1 and 2. The Monte Carlo analysis produced two fits to each of 10,000 simulated datasets generated from re-sampling the distribution of residuals; the set of simulated datasets estimates the uncertainty in the measured values on the y-axis (i.e., $\ln(K_1/K_{1Ref})$ and $\ln(K_2/K_{2Ref})$). The fit with ΔC_p set to zero (red line) produces a straight line with zero curvature, and yields curved residuals for steps 1 and 2 (right plots). This curvature is reduced when ΔC_p is non-zero (blue line).

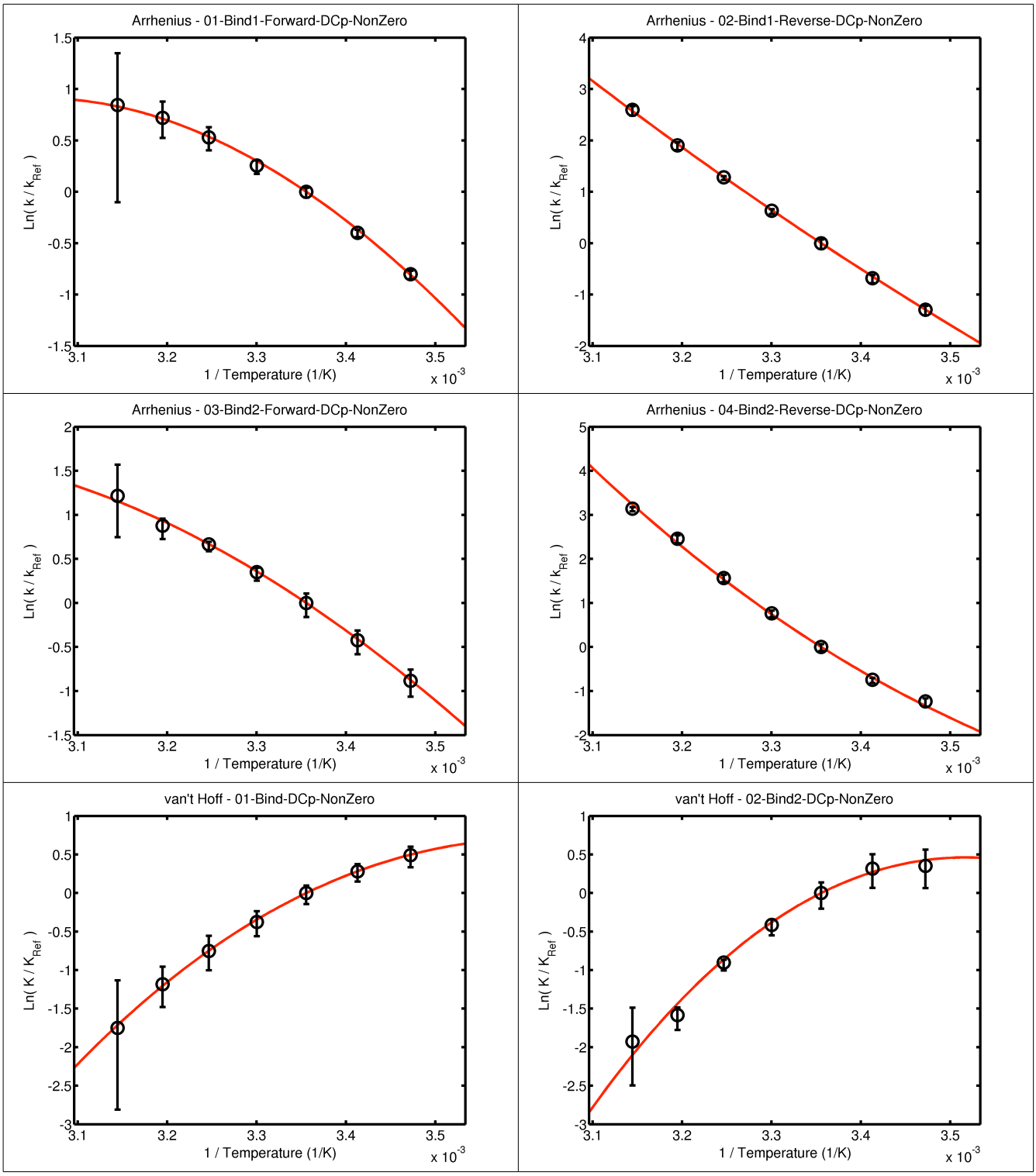

Figure S6. Data at 45°C were not used in the temperature-dependent Arrhenius and van't Hoff analyses because the two forward rate constants yielded Arrhenius and van't Hoff quantities that were outlying

with large uncertainties (45°C is the left-most point in each figure). The red line shows a fit to either the extended Arrhenius or the extended van't Hoff equation (i.e., $\Delta C_p^{\ddagger}$ or ΔC_p is non-zero). Error bars are 95% confidence intervals from a Monte Carlo error analysis propagated from the original stopped flow time courses.

Supporting Tables

Table S1. Sum of squared error (SSE) for comparing models A [BB] and B [BI].

		15ºC	20ºC	25ºC	30ºC	35ºC	40ºC	45ºC	All (15-45ºC)
SSE	**Model A [BB]**	1.000	1.000	1.000	1.000	1.000	1.000	1.002	7.002
	Model B [BI]	1.527	1.928	2.324	2.665	2.100	1.288	1.000	12.832

Model A [BB] is favored over model B [BI] because it has the same number of fitting parameters and its fits exhibit lower SSE at 15-40ºC, whereas it has equivalent SSE to model B [BI] at 45ºC. SSE values are normalized within each temperature so that the sum in the right-most column weights each temperature equally.

Table S2. Fitted parameters to k^{obs} vs. TRAP concentration.

	K^{obs} From Two-Phase Exponential	K^{obs} From Three-Phase Exponential
15ºC	k_1^f = 0.23 [0.06] k_1^b = 1.13 [0.30] K_d = 5.13 [3.07] k_2^f = 0.22 [0.04] k_2^b = 0.03 [0.02]	k_1^f = 0 [Undefined] k_1^b = 4.31 [1.30] K_{d2} = 7.59 [30.96] k_2^f = 1.37 [2.17] k_2^b = 0.76 [0.48] K_{d3} = 0.75 [3.39] k_3^f = 0.12 [0.19] k_3^b = 0.002 [0.22]
20ºC	k_1^f = 0.36 [0.05] k_1^b = 1.95 [0.28] K_d = 3.56 [0.90] k_2^f = 0.27 [0.01] k_2^b = 0.04 [0.01]	k_1^f = 0.33 [0.22] k_1^b = 3.49 [1.25] K_{d2} = 2.91e5 [1.41e10] k_2^f = 6.59e5 [3.19e9] k_2^b = 0.71 [0.92] K_{d3} = 2.40 [0.60] k_3^f = 0.18 [0.01] k_3^b = 0.04 [0.01]
25ºC	k_1^f = 0.52 [0.04] k_1^b = 3.64 [0.22] K_d = 3.50 [2.32] k_2^f = 0.33 [0.06] k_2^b = 0.07 [0.05]	k_1^f = 0.46 [0.15] k_1^b = 5.16 [0.83] K_{d2} = 76.05 [4.57e3] k_2^f = 9.50 [4.98e2] k_2^b = 1.35 [1.90] K_{d3} = 2.67 [4.17]

		k_3^f = 0.27 [0.07] k_3^b = 0.08 [0.09]
30ºC	k_1^f = 0.75 [0.08] k_1^b = 6.54 [0.44] K_d = 4.14 [1.17] k_2^f = 0.71 [0.05] k_2^b = 0.12 [0.03]	k_1^f = 0.84 [0.20] k_1^b = 7.72 [1.17] K_{d2} = 6.23 [16.01] k_2^f = 6.56 [8.33] k_2^b = 0 [Undefined] K_{d3} = 2.56 [3.74] k_3^f = 0.54 [0.13] k_3^b = 0.06 [0.16]
35ºC	k_1^f = 0.89 [0.30] k_1^b = 13.57 [1.73] K_d = 7.59 [3.53] k_2^f = 1.22 [0.22] k_2^b = 0.32 [0.05]	k_1^f = 0 [Undefined] k_1^b = 24.55 [6.46] K_{d2} = 0.25 [35.07] k_2^f = 2.86 [2.71e2] k_2^b = 2.73 [2.77e2] K_{d3} = 2.07 [3.68] k_3^f = 0.70 [0.21] k_3^b = 0.18 [0.30]
40ºC	k_1^f = 1.47 [0.59] k_1^b = 22.12 [3.39] K_d = 3.69 [4.60] k_2^f = 1.48 [0.39] k_2^b = 0.54 [0.29]	k_1^f = 0 [5.91] k_1^b = 38.55 [33.70] K_{d2} = 0 [Undefined] k_2^f = 0 [Undefined] k_2^b = 13.21 [10.38] K_{d3} = 27.00 [2.20e2] k_3^f = 2.30 [13.29]

		k_3^b = 0.75 [0.34]
45ºC	k_1^f = 1.59 [1.48] k_1^b = 46.09 [8.45] K_d = 26.13 [264.33] k_2^f = 3.19 [22.62] k_2^b = 1.66 [0.61]	k_1^f = 0 [Undefined] k_1^b = 79.21 [30.24] K_{d2} = 0.03 [1.06e8] k_2^f = 9e-6 [3.44e4] k_2^b = 12.00 [3.44e4] K_{d3} = 0.45 [0.62] k_3^f = 1.74 [0.43] k_3^b = 0 [Undefined]

Parameters from fitting the concentration-dependence of the mechanism-independent apparent rate constants to either a two-phase or three-phase exponential equation. Fit results are shown in Fig S2. The units of each number are as follows: k_1^f, k_2^f, and k_3^f are /μM/sec, k_1^b, k_2^b, and k_3^b are /sec, and K_d, K_d^2, and K_d^3 are μM. The values in brackets are standard fitting errors from MATLAB, where "Undefined" means MATLAB could not successfully determine the fitted value and/or its error.

Table S3. Bayesian Information Criterion (BIC) for comparing fits of stopped-flow data to 2-, 3-, and 4-phase exponential equations.

Name	2-Exp BIC Weight	3-Exp BIC Weight	4-Exp BIC Weight	Best Model
15C-t1	0.062	0.935	0.003	3
15C-t2	0.071	0.926	0.003	3
15C-t3	0	0.974	0.026	3
15C-t4	0	0.997	0.003	3
15C-t5	0	0.997	0.003	3
15C-t7	0	0.997	0.003	3
20C-t1	0.955	0.045	0	2
20C-t2	0.236	0.759	0.004	3
20C-t3	0.009	0.98	0.011	3
20C-t4	0	0.839	0.161	3
20C-t5	0	0.963	0.037	3
20C-t6	0	0.959	0.041	3
20C-t7	0	0.93	0.07	3
25C-t1	0.976	0.024	0	2
25C-t2	0.958	0.042	0	2
25C-t3	0.005	0.989	0.006	3
25C-t4	0	0.993	0.007	3
25C-t5	0	0.974	0.026	3
25C-t6	0	0.517	0.483	3
25C-t7	0	0.103	0.897	4
30C-t1	0.884	0.116	0	2
30C-t2	0.667	0.091	0.243	2
30C-t3	0	0.996	0.003	3
30C-t4	0.002	0.956	0.042	3
30C-t5	0	0.938	0.062	3
30C-t6	0	0.974	0.026	3
30C-t7	0	0.997	0.003	3
35C-t1	0.574	0.424	0.002	2
35C-t2	0.103	0.894	0.003	3
35C-t3	0.006	0.994	0	3
35C-t4	0.001	0.983	0.016	3
35C-t5	0	0.922	0.078	3
35C-t6	0	0.862	0.138	3
35C-t7	0	0.587	0.413	3
40C-t1	0.993	0.007	0	2
40C-t2	0.983	0.017	0	2
40C-t3	0.993	0.007	0	2
40C-t4	0.007	0.99	0.003	3
40C-t5	0.026	0.966	0.009	3
40C-t6	0.002	0.99	0.008	3
40C-t7	0	0.992	0.007	3
45C-t1	0.985	0.015	0	2
45C-t2	0.574	0.425	0	2
45C-t3	0.234	0.764	0.003	3
45C-t4	0.001	0.985	0.015	3
45C-t5	0.021	0.97	0.009	3
45C-t6	0.002	0.987	0.011	3

The 3-phase model is generally preferred as it has the largest BIC at each temperature and TRAP concentration. Fits are shown in figure S1.

References

1. Kuzmic, P. (1996) Program dynafit for the analysis of enzyme kinetic data: application to hiv proteinase, *Anal. Biochem.* 237, pp. 260-273.

2. Kuzmic, P. (2009) Dynafit--a software package for enzymology., *Meth. Enzymol.* 467, pp. 247-280.